3836 *Inorg. Chem.* **2010**, *49*, 3836–3850
DOI: 10.1021/ic902550g

Inorganic Chemistry
Article

Gas-Phase Reactions of Uranate Ions, UO_2^-, UO_3^-, UO_4^-, and UO_4H^-, with Methanol: a Convergence of Experiment and Theory

Maria del Carmen Michelini,*,† Joaquim Marçalo,‡ Nino Russo,† and John K. Gibson*,§

†*Dipartimento di Chimica, Università della Calabria, Via P. Bucci, Cubo 14 C, 87030 Arcavacata di Rende, Italy,* ‡*Unidade de Ciências Químicas e Radiofarmacêuticas, Instituto Tecnológico e Nuclear, 2686-953 Sacavém, Portugal, and* §*Chemical Sciences Division, Lawrence Berkeley National Laboratory, Berkeley, California 94720*

Received December 21, 2009

Bimolecular reactions of uranium oxide molecular anions with methanol have been studied experimentally, by Fourier transform ion cyclotron resonance mass spectrometry, and computationally, by density functional theory (DFT). The primary goals were to provide fundamental insights into mechanistic and structural details of model reactions of uranium oxides with organics, and to examine the validity of theoretical modeling of these types of reactions. The ions UO_3^-, UO_4^-, and UO_4H^- each reacted with methanol to give a singular product; the primary products each exhibited sequential reactions with two additional methanol molecules to again give singular products. The observed reactions were elimination of water, formaldehyde, or hydrogen, and in one case addition of a methanol molecule. The potential energy profiles were computed for each reaction, and isotopic labeling experiments were performed to probe the validity of the computed mechanisms and structures—in each case where the experiments could be compared with the theory there was concurrence, clearly establishing the efficacy of the employed DFT methodologies for these and related reaction systems. The DFT results were furthermore in accord with the surprisingly inert nature of UO_2^-. The results provide a basis to understand mechanisms of key reactions of uranium oxides with organics, and a foundation to extend DFT methodologies to more complex actinide systems which are not amenable to such direct experimental studies.

Introduction

Reactions of bare and ligated transition metal ions with neutral molecules in the gas phase have been systematically studied for more than 30 years, as described in a number of reviews.[1−8] These efforts have provided key thermochemical values, particularly bond dissociation energies, as well as fundamental insights into reaction mechanisms at a molecular level. A key advantage of gas-phase reactivity studies is the relative simplicity of the chemical interactions between two isolated species; this contrasts with the complexities introduced by perturbations intrinsic to condensed phase chemistry. This attribute of bimolecular simplicity provides an opportunity to probe discrete chemical interactions between two species, and is well-suited to advanced computational modeling.

Much of the early work in this field focused on d-block transition metals, particularly the 3d series.[9,10] Moreland et al. were among the first to study gas-phase actinide ion reactions, specifically reactions of U^+ and Pu^+ with water and hydrogen to produce the actinide hydride ions.[11] Johnsen and Biondi subsequently carried out a systematic study of the oxidation of U^+ by O_2.[12] Later, Armentrout and Beauchamp studied reactions of the U^+ ion with several elementary molecules.[13−15] Since this pioneering work, studies of gas-phase actinide ion chemistry have been performed by a variety of techniques, and have been applied to the actinides from thorium through einsteinium, as described in recent reviews.[16−18]

*To whom correspondence should be addressed. E-mail: mc.michelini@unical.it (M.C.M.), jkgibson@lbl.gov (J.K.G.).

(1) Armentrout, P. B.; Beauchamp, J. L. *Acc. Chem. Res.* **1989**, *22*, 315–321.
(2) Armentrout, P. B. In *Gas phase Inorganic Chemistry*; Russell, D. H., Ed.; Plenum Press: New York, 1989, pp 1−42.
(3) Eller, K.; Schwarz, H. *Chem. Rev.* **1991**, *91*, 1121–1177.
(4) Freiser, B. S. *Acc. Chem. Res.* **1994**, *27*, 353–360.
(5) Freiser, B. S. *J. Mass Spectrom.* **1996**, *31*, 703–715.
(6) Schwarz, H. *Angew. Chem., Int. Ed.* **2003**, *42*, 4442–4454.
(7) Armentrout, P. B. *Int. J. Mass Spectrom.* **2003**, *227*, 289–302.
(8) Böhme, D. K.; Schwarz, H. *Angew. Chem., Int. Ed.* **2005**, *44*, 2336–2354.
(9) Armentrout, P. B.; Kickel, B. L. In *Organometallic Ion Chemistry*; Freiser, B. S., Ed.; Kluwer: Dordrecht, The Netherlands, 1995, pp 1−45.
(10) Armentrout, P. B. In *The Encyclopedia of Mass Spectrometry*; Armentrout, P. B., Ed.; Elsevier: Boston, 2003; Vol. *1*, pp 800−810.
(11) Moreland, P. E.; Rokop, D. J.; Stevens, C. M. *Int. J. Mass Spectrom. and Ion Phys.* **1970**, *5*, 127–136.
(12) Johnsen, R.; Biondi, M. A. *J. Chem. Phys.* **1972**, *57*, 1975–1979.
(13) Armentrout, P.; Hodges, R.; Beauchamp, J. L. *J. Am. Chem. Soc.* **1977**, *99*, 3162–3163.
(14) Armentrout, P. B.; Beauchamp, J. L. *Chem. Phys.* **1980**, *50*, 27–36.
(15) Armentrout, P. B.; Beauchamp, J. L. *J. Phys. Chem.* **1981**, *85*, 4103–4105.
(16) Gibson, J. K. *Int. J. Mass Spectrom.* **2002**, *214*, 1–21.
(17) Gibson, J. K.; Marçalo, J. *Coord. Chem. Rev.* **2006**, *250*, 776–783.
(18) Heaven, M. C.; Gibson, J. K.; Marçalo, J. In *The Chemistry of the Actinide and Transactinide Elements*; Morss, L. R., Edelstein, N. M., Fuger, J., Eds.; Springer: Dordrecht, The Netherlands, 2010, in press.

 Published on Web 03/17/2010

Gas-phase metal ion chemistry is often presented as a route to understanding condensed phase chemistry, so it is crucial to recognize the clear limitations of drawing comparisons between these disparate states of matter.[18,19] Nonetheless, it has been well established that reactions studied under rarefied gas-phase conditions can provide important fundamental insights into molecular processes, such as catalysis and surface chemistry.[8,20−30] A central goal of chemistry is to understand the dynamics which occur during reactions. However, it is experimentally very challenging to directly probe the dynamics of chemical reactions.[31−33] An alternative approach for bimolecular reactions in the gas phase is to analyze the details of reaction pathways by computational chemistry; the computed mechanisms can often be directly compared with experimental observations, such as reaction kinetics, and product distributions and structures. The use of Density Functional Theory (DFT) to compute such bimolecular reaction mechanisms has become widespread. Cramer[34] has described such applications of DFT, including a discussion of the theoretical characterization of the catalytic carbonylation of methanol reported by Kinnunen and Laasonen.[35] A few recent examples of applications of DFT to gas-phase chemistry include reactions of carbonyl oxides with ammonia,[36] of N with NCO,[37] of CF_3O with CO,[38] and of La/La^+ with CO_2.[39]

The proton-rich actinide elements, which as neutral atoms have from 89 (Ac) to 103 (Lr) electrons, have presented a particular challenge to molecular theory methods, as reviewed by Pepper and Bursten in 1991.[40] In the intervening years, great advances in applications of DFT methods to actinide molecular systems have been achieved[41] to the extent that such applications have become widespread and generally reliable, if often rather computationally intensive.[42−45] DFT has recently been employed to describe reactions of gas-phase actinide ions with small molecules;[46−50] the detailed computed reaction pathways effectively concurred with experimental observations, which had been previously reported, thereby validating the DFT methods for these types of computations. In a very recent paper, Zhou and Schlegel[51] have reported a detailed study of the $Th^+ + H_2O$ reaction, using DFT and Coupled Clusters methods; the authors used molecular dynamic simulations to determine the products' branching ratio.

The goal of the work reported here was to examine a model set of ion/molecule reactions in the gas phase, both experimentally and theoretically. By carrying out the two parallel aspects of the project—experiment and theory—in close cooperation, it was possible to devise isotopic labeling experiments to assess specific aspects of the computed reaction mechanisms and reactant ion structures. The model systems studied were the reactions between the elementary uranium oxide anions, UO_2^-, UO_3^-, UO_4^-, and UO_4H^-, and the elementary alcohol, methanol. The choice of the uranium oxide anions, which we refer to as "uranates" in analogy with condensed phase chemistry, provides an opportunity to understand uranium oxide chemistry at a molecular level, and was facilitated by our ability to produce these species in abundance.[52] The very elementary organic methanol reactant is of particular interest for such reaction mechanism studies because of the importance of reactions of organic materials with uranium oxides in various technological and geological scenarios, which have motivated several experimental studies of reactions of small organic molecules with uranium oxide surfaces, primarily by Idriss and coworkers.[53−61] Lloyd et al. studied the reaction of methanol with uranium dioxide surfaces,[62] which is particularly relevant

(19) Fisher, K. J.; Dance, I. G.; Willett, G. D. *Rapid Commun. Mass Spectrom.* **1996**, *10*, 106–109.
(20) Squires, R. R. *Chem. Rev.* **1987**, *87*, 623–646.
(21) Deng, H. T.; Kerns, K. P.; Castleman, A. W. *J. Phys. Chem.* **1996**, *100*, 13386–13392.
(22) Keesee, R. G.; Chen, B.; Harms, A. C.; Castleman, A. W. *Int. J. Mass Spectrom. Ion Processes* **1993**, *123*, 225–231.
(23) Zemski, K. A.; Bell, R. C.; Castleman, A. W. *Int. J. Mass Spectrom.* **1999**, *184*, 119–128.
(24) Zemski, K. A.; Bell, R. C.; Castleman, A. W. *J. Phys. Chem. A* **2000**, *104*, 5732–5741.
(25) Zemski, K. A.; Justes, D. R.; Bell, R. C.; Castleman, A. W. *J. Phys. Chem. A* **2001**, *105*, 4410–4417.
(26) Zemski, K. A.; Justes, D. R.; Castleman, A. W. *J. Phys. Chem. B* **2002**, *106*, 6136–6148.
(27) O'Hair, R. A. J.; Khairallah, G. N. *J. Cluster Sci.* **2004**, *15*, 331–363.
(28) Jena, P.; Castleman, A. W. *Proc. Natl. Acad. Sci. U.S.A.* **2006**, *103*, 10560–10569.
(29) Wyrwas, R. B.; Yoder, B. L.; Maze, J. T.; Jarrold, C. C. *J. Phys. Chem. A* **2006**, *110*, 2157–2164.
(30) Mayhall, N. J.; Raghavachari, K. *J. Phys. Chem. A* **2007**, *111*, 8211–8217.
(31) Zare, R. N. *Science* **2006**, *311*, 1383–1385.
(32) Chapman, H. N.; et al. *Nature* **2007**, *448*, 676–679; see ref 36. of the Supporting Information for full citation.
(33) Cahoon, J. F.; Sawyer, K. R.; Schlegel, J. P.; Harris, C. B. *Science* **2008**, *319*, 1820–1823.
(34) Cramer, C. J. *Essentials of Computational Chemistry*, 2nd ed.; Wiley: Chichester, 2004.
(35) Kinnunen, T.; Laasonen, K. *J. Organomet. Chem.* **2001**, *628*, 222–232.
(36) Jorgensen, S.; Gross, A. *J. Phys. Chem. A* **2009**, *113*, 10284–10290.
(37) Zuo, M. H.; Liu, H. L.; Huang, X. R.; Sun, C. C.; Tang, A. C. *J. Theor. Comput. Chem.* **2009**, *8*, 587–595.
(38) Xu, G. H.; Shen, C. Y.; Han, H. Y.; Li, J. Q.; Wang, H. M.; Chu, Y. N. *J. Mol. Struct.: THEOCHEM* **2009**, *910*, 34–40.
(39) Dai, G. L.; Wang, C. F. *J. Mol. Struct.: THEOCHEM* **2009**, *909*, 122–128.
(40) Pepper, M.; Bursten, B. E. *Chem. Rev.* **1991**, *91*, 719–741.
(41) Schreckenbach, G.; Hay, P. J.; Martin, R. L. *J. Comput. Chem.* **1999**, *20*, 70–90.
(42) Garcia-Hernandez, M.; Willnauer, C.; Krüger, S.; Moskaleva, L. V.; Rösch, N. *Inorg. Chem.* **2006**, *45*, 1356–1366.
(43) Denning, R. G. *J. Phys. Chem. A* **2007**, *111*, 4125–4143.
(44) Gagliardi, L.; Roos, B. O. *Chem. Soc. Rev.* **2007**, *36*, 893–903.
(45) Arliguie, T.; Belkhiri, L.; Bouaoud, S. E.; Thuery, P.; Villiers, C.; Boucekkine, A.; Ephritikhine, M. *Inorg. Chem.* **2009**, *48*, 221–230.
(46) Michelini, M. C.; Russo, N.; Sicilia, E. *Angew. Chem., Int. Ed.* **2006**, *118*, 1113–1117.
(47) Michelini, M. C.; Russo, N.; Sicilia, E. *J. Am. Chem. Soc.* **2007**, *129*, 4229–4239.
(48) Alikhani, M. E.; Michelini, M. C.; Russo, N.; Silvi, B. *J. Phys. Chem. A* **2008**, *112*, 12966–12974.
(49) Di Santo, E.; Michelini, M. C.; Russo, N. *Organometallics* **2009**, *28*, 3716–3726.
(50) Di Santo, E.; Michelini, M. C.; Russo, N. *J. Phys. Chem. A* **2009**, *113*, 14699–14705.
(51) Zhou, J.; Schlegel, H. B. *J. Phys. Chem. A* **2010**, DOI: 10.1021/jp912098w.
(52) Marçalo, J.; Santos, M.; Pires de Matos, A.; Gibson, J. K. *Inorg. Chem.* **2009**, *48*, 5055–5057.
(53) Madhavaram, H.; Buchanan, P.; Idriss, H. *J. Vac. Sci. Technol., A* **1997**, *15*, 1685–1691.
(54) Madhavaram, H.; Idriss, H. *J. Catal.* **1999**, *184*, 553–556.
(55) Chong, S. V.; Idriss, H. *J. Vac. Sci. Technol., A* **2000**, *18*, 1900–1905.
(56) Madhavaram, H.; Idriss, H. *Catal. Today* **2000**, *63*, 309–315.
(57) Chong, S. V.; Griffiths, T. R.; Idriss, H. *Surf. Sci.* **2000**, *444*, 187–198.
(58) Madhavaram, H.; Idriss, H. *J. Catal.* **2002**, *206*, 155–158.
(59) Senanayake, S. D.; Chong, S. V.; Idriss, H. *Catal. Today* **2003**, *85*, 311–320.
(60) King, R. I.; Senanayake, S. D.; Chong, S. V.; Idriss, H. *Surf. Sci.* **2007**, *601*, 5690–5700.
(61) King, R.; Idriss, H. *Langmuir* **2009**, *25*, 4543–4555.
(62) Lloyd, J. A.; Manner, W. L.; Paffett, M. T. *Surf. Sci.* **1999**, *423*, 265–275.

to the gas-phase studies reported here. There have been several studies of gas-phase reactions of metal oxide ions with methanol, largely to understand fundamental aspects of catalytic processes.[63−74]

Here we present results for the bimolecular reactions of UO_x^- ($x = 2-4$) and UO_4H^- anions with CH_3OH, along with secondary and tertiary reactions of the primary product ions with additional methanol molecules. The experimental observations, particularly with isotopically labeled methanol reagent molecules, are used to evaluate the validity of reaction pathways computed by DFT. The results are compared with previous results for reactions of methanol with metal oxides in both the gas phase and at interfaces. By the close interplay between experiment and theory, we have achieved an understanding of mechanistic details of these gas-phase reactions.

Methods

Computational Details. The details of the theoretical approach used in this work have been previously reported.[46−50] We have included a detailed description of the methodology in the Supporting Information. In this section we briefly summarize the methods.

Geometry optimizations as well as frequency calculations for all the reactants, intermediates, products, and transition states were performed using two different approaches of DFT. First, the Zero−Order Regular Approximation (ZORA) was used in combination with the PW91 functionals (exchange and correlation)[75−79] and the TZ2P (TZP for uranium) basis set, as implemented in the ADF package[80−82] (we refer to this level of theory as PW91/ZORA hereafter). Second, the hybrid B3LYP functional[83,84] was employed together with the Stuttgart−Dresden basis sets for the metal center,[85,86] (25s 16p 15d 7f)/[7s 6p 5d 3f] in combination with the small-core relativistic effective core potential (RECP). The B3LYP/SDD (SDD = Stuttgart−Dresden relativistic effective core potential) computations were carried out with GAUSSIAN03 package.[87] Spin−orbit effects were not treated explicitly in this work.

We report the potential energy profiles (PEPs) for each of the studied reactions as relative energies (electronic energies + ZPVE at 0 K) of each species with respect to the ground state reactants. All the reported structures and PEPs involved in the reaction sequences 1 and 2 (UO_3^- and UO_4^-; see Scheme 1), as well as the studied reactions of UO_2^- with methanol, correspond to the doublet ground spin state whereas in the reaction sequence 3 (UO_4H^-, see Scheme 1) all the species are in their singlet ground spin state.

Experimental Section. The experimental approach has been described previously.[65,88−90] A brief outline of the general approach is included here—the experimental details are in the Supporting Information. Uranium oxide (hydroxide) anions were produced by laser desorption ionization of solids. Bimolecular gas-phase reactions of methanol with the primary anions, and sequential anion products, were studied by Fourier transform ion cyclotron resonance mass spectrometry. Pseudo first-order reaction kinetics were determined by isolating and cooling anions, and measuring the time-dependence of the decay of reactant ions and the in-growth of product ions. Along with the absolute rate constants, and for comparative purposes, reaction efficiencies are reported as k/k_{COL}, where the k_{COL} is the collisional rate constant derived from the modified variational transition-state/classical trajectory theory developed by Su and Chesnavich.[91] Reaction pathways were examined using methanols isotopically labeled with deuterium or oxygen-18. Fragmentation of isolated product ions was studied by collision induced dissociation (CID), in which a specific ion is excited by an rf pulse and collided with argon.

Results and Discussion

The theoretical descriptions of the mechanisms for the observed uranate methanol reactions, as well as product structures, were evaluated from the experimental results for the isotopically substituted methanol molecules. Accordingly, the experimental reactivity results for unlabeled CH_3OH with the three uranate ions are presented, followed by the corresponding theoretical results, and finally the experimental results for the reactions with the CD_3OH, CD_3OD, and $CH_3{}^{18}OH$ isotopologues, including kinetic isotope effects and CID of selected product ions.

Experimental Results for Uranates with CH_3OH. Three of the uranate ions, UO_3^-, UO_4^-, and UO_4H^-, sequentially reacted with three methanol molecules. These three reaction sequences are summarized in Scheme 1. Each of these reactions yielded only one product ion to within an estimated sensitivity of $<1\%$. The indicated terminal product ions were inert toward further reaction with methanol to within

(63) Fialko, E. F.; Kikhtenko, A. V.; Goncharov, V. B.; Zamaraev, K. I. *J. Phys. Chem. B* **1997**, *101*, 5772–5773.
(64) Fialko, E. F.; Kikhtenko, A. V.; Goncharov, V. B. *Organometallics* **1998**, *17*, 25–31.
(65) Oliveira, M. C.; Marçalo, J.; Vieira, M. C.; Ferreira, M. A. A. *Int. J. Mass Spectrom.* **1999**, *187*, 825–835.
(66) Jackson, P.; Fisher, K. J.; Willett, G. D. *Int. J. Mass Spectrom.* **2000**, *197*, 95–103.
(67) Jackson, P.; Fisher, K. J.; Willett, G. D. *Chem. Phys.* **2000**, *262*, 179–187.
(68) Waters, T.; O'Hair, R. A. J.; Wedd, A. G. *J. Am. Chem. Soc.* **2003**, *125*, 3384–3396.
(69) Justes, D. R.; Moore, N. A.; Castleman, A. W. *J. Phys. Chem. B* **2004**, *108*, 3855–3862.
(70) Cao, Y. L.; Zhao, X. A.; Xin, B.; Xiong, S. X.; Tang, Z. C. *J. Mol. Struct.: THEOCHEM* **2004**, *683*, 141–146.
(71) Jackson, P.; Fisher, K. J.; Willett, G. D. *Phys. Chem. Chem. Phys.* **2005**, *7*, 1687–1693.
(72) Feyel, S.; Scharfenberg, L.; Daniel, C.; Hartl, H.; Schröder, D.; Schwarz, H. *J. Phys. Chem. A* **2007**, *111*, 3278–3286.
(73) Waters, T.; Wedd, A. G.; O'Hair, R. A. J. *Chem.—Eur. J.* **2007**, *13*, 8818–8829.
(74) Dong, F.; Heinbuch, S.; Xie, Y.; Rocca, J. J.; Bernstein, E. R. *J. Phys. Chem. A* **2009**, *113*, 3029–3040.
(75) Perdew, J. P. In *Electronic Structure of Solids '91*; Ziesche, P., Eschring, H., Eds.; Akademie-Verlag: Berlin, Germany, 1991; p 11.
(76) Perdew, J. P.; Chevary, J. A.; Vosko, S. H.; Jackson, K. A.; Pederson, M. R.; Singh, D. J.; Fiolhais, C. *Phys. Rev. B* **1992**, *46*, 6671–6687.
(77) Perdew, J. P.; Chevary, J. A.; Vosko, S. H.; Jackson, K. A.; Pederson, M. R.; Singh, D. J.; Fiolhais, C. *Phys. Rev. B* **1993**, *48*, 4978–4978.
(78) Perdew, J. P.; Burke, K.; Wang, Y. *Phys. Rev. B* **1996**, *54*, 16533.
(79) Burke, K.; Perdew, J. P.; Wang, Y. In *Electronic Density Functional Theory: Recent Progress and New Directions*; Dobson, J. F., Vignale, G., Das, M. P., Eds.; Plenum: New York, 1998.
(80) Fonseca Guerra, C.; Snijders, J. G.; te Velde, G.; Baerends, E. J. *Theor. Chem. Acc.* **1998**, *99*, 391–403.
(81) te Velde, G.; Bickelhaupt, F. M.; van Gisbergen, S. J. A.; Fonseca Guerra, C.; Baerends, E. J.; Snijders, J. G.; Ziegler, T. *J. Comput. Chem.* **2001**, *22*, 931–967.
(82) *ADF2004.01 SCM*; Theoretical Chemistry, Vrije Universiteit: Amsterdam, The Netherlands, 2004; http://www.scm.com.
(83) Becke, A. D. *J. Chem. Phys.* **1993**, *98*, 5648–5652.
(84) Lee, C. T.; Yang, W. T.; Parr, R. G. *Phys. Rev. B* **1988**, *37*, 785–789.
(85) Kuchle, W.; Dolg, M.; Stoll, H.; Preuss, H. *J. Chem. Phys.* **1994**, *100*, 7535–7542.
(86) http://www.theochem.unistuttgart.de/pseudopotentiale/.
(87) Frisch, M. J. et al. *Gaussian 03*, Revision C02; Gaussian,Inc.: Wallingford, CT, 2004; eee Supporting Information for full citation.
(88) Marçalo, J.; Leal, J. P.; Pires de Matos, A.; Marshall, A. G. *Organometallics* **1997**, *16*, 4581–4588.
(89) Santos, M.; Marçalo, J.; Pires de Matos, A.; Gibson, J. K.; Haire, R. G. *J. Phys. Chem. A* **2002**, *106*, 7190–7194.
(90) Marçalo, J.; Santos, M.; Pires de Matos, A.; Gibson, J. K.; Haire, R. G. *J. Phys. Chem. A* **2008**, *112*, 12647–12656.
(91) Su, T.; Chesnavich, W. J. *J. Chem. Phys.* **1982**, *76*, 5183–5185.

Scheme 1[a]

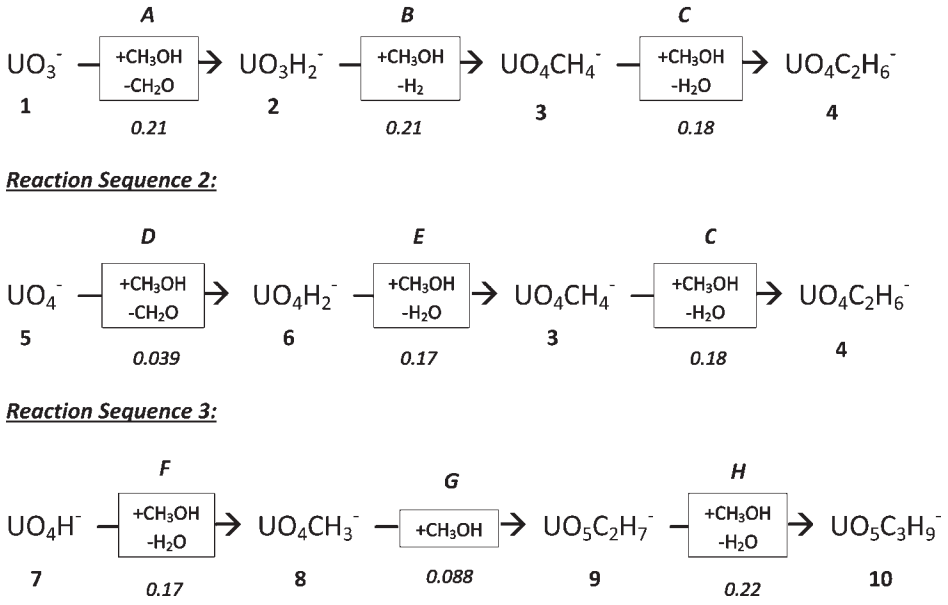

[a] k/k_{COL} values are given in italics.

the detection limit, $k/k_{COL} < 0.001$. The primary reactant ions, intermediate product ions, and terminal products ions are designated as **1**, **2**, **3**, and so forth; the reactions are designated as ***A***, ***B***, ***C***, and so forth. Also included in Scheme 1, in italics, are the reaction efficiencies, k/k_{COL}. Implicit in Scheme 1 is that the tertiary product **3** with the composition $UO_4CH_4^-$ is the same in sequences ***1*** and ***2***. The identical kinetics, that is, $k/k_{COL} = 0.18$, for the subsequent reactions of these two $UO_4CH_4^-$ products substantiates this conclusion, as do other theoretical and experimental results discussed below. The absolute pseudo-first order rate constants, as well as the k/k_{COL} values included in Scheme 1, are compiled in Table 1. Representative kinetics data are shown for reactions ***A***, ***D***, and ***F*** in Supporting Information, Figures S1, S2 and S3, respectively; also given there are the measured reactant depletion rates, the methanol pressures, and the resulting pseudo-first order rate constants. The observed reactions are discussed in detail below in the comparison of the computed reaction mechanisms with experimental results for the isotopically substituted methanol molecules.

The UO_2^- ion was found to be unreactive with methanol to within the detection limit of the experiments, $k/k_{COL} < 0.001$. This intriguing observation is discussed below, along with computed reaction pathways for some hypothetical UO_2^-/CH_3OH reactions.

Computed Structures. (a). Primary Uranate Ions. The computed structures of the four primary uranate ions are shown in Figure 1, with the geometrical parameters given at both levels of theory; also included are the geometrical parameters and energies relative to the ground-state of two higher-energy isomers of UO_4^-. The uranium−oxygen bond distances and computed charges (Natural Population Analysis) at the uranium metal center and the oxygen atoms are given in Table S1 (Supporting Information) for the three binary UO_x^- ($x = 2, 3, 4$) along with the corresponding values for some cationic and neutral uranium oxide molecules, several of which were studied previously using the same DFT methodology employed in the present work.[46,47] The UO_2^- ion is linear like uranyl, UO_2^{2+}, with the bond distance elongated by ~0.1 Å relative to the dipositive ion. The other three uranate ions, UO_3^-, UO_4^-, and UO_4H^-, each appear to retain the core uranyl moiety, albeit somewhat distorted from linearity, by ~20°, and with the U−O bonds slightly elongated, by < 0.1 Å.

Table 1. Kinetics for Reactions with CH_3OH[a]

	k[b]	k/k_{COL}
A	0.36	0.21
B	0.37	0.21
C	0.30[c]	0.18
D	0.067	0.039
E	0.29	0.17
F	0.29	0.17
G	0.15	0.088
H	0.38	0.22

[a] The reactions are identified in Scheme 1. [b] Pseudo-first-order rate constants, k, are in units of 10^{-9} cm^3 molecule^{-1} s^{-1}. [c] This is the rate constant for ***C*** measured in reaction sequence 1; the value measured in reaction sequence 2 was 0.31×10^{-9} cm^3 molecule^{-1} s^{-1}, which is essentially identical.

The low-symmetry tetrakis-oxo structure of UO_4^- is particularly intriguing in that it comprises four discrete U−O bonds with a single negative charge on the species such that the *formal* oxidation state at the metal center is U(VII). We note, however, that in contrast to UO_3^-, in which the unpaired electron is localized on a 5f uranium orbital (Natural Bond Orbital Analysis), in the case of UO_4^- the unpaired electron and, therefore, the radical character is delocalized between the two "equatorial" oxygen atoms. As shown in Figure 1, both the "side on" $(\eta^2\text{-}O_2)UO_2^-$ and the end on $(\eta^1\text{-}O_2)UO_2^-$ structures which incorporate a dioxo moiety are computed to lie at substantially higher energies. The "uranyl" moiety is evident in UO_4^-, with the bond lengths and angles similar to those in UO_3^- and UO_4H^-. The two equatorial U−O

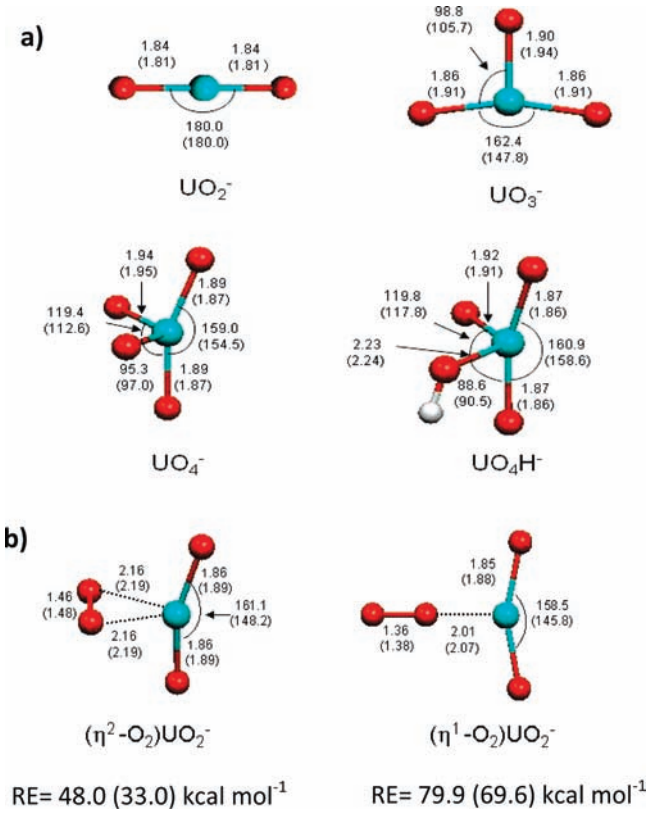

Figure 1. (a) Geometrical parameters for the reactants, UO_2^-, UO_3^-, UO_4^-, and UO_4H^-, at PW91/ZORA (B3LYP/SDD) level of theory. Bond lengths are in Å and angles are in degrees. (b) Geometrical parameters and energies relative to the ground-state isomer for the two high-energy isomers of UO_4^-.

bonds are slightly longer than the "uranyl" U−O bonds in UO_4^- but are much shorter than the U−OH bond in UO_4H^-. The somewhat remarkable low-energy structure of UO_4^- can be compared with those of related species. Groenewold et al. observed that O_2 binds to UO_2^+ in the gas phase;[92] subsequent theoretical computations[93,94] indicated that the resulting UO_4^+ ion is a "superoxo" $(\eta^2\text{-}O_2)UO_2^+$ species, with a structure similar to that shown for the corresponding high-energy UO_4^- isomer in Figure 1b; the $(\eta^1\text{-}O_2)UO_2^+$ structure was computed to be at least 10 kcal mol^{-1} higher in energy (the energy of the tetrakis-oxo structure was not provided). Aubriet et al.[95] computed the lowest energy structure of CeO_4^- as $(\eta^2\text{-}O_2)CeO_2^-$ and found the tetrakis-oxo tetrahedral CeO_4^- isomer to be 62 kcal mol^{-1} higher in energy. Bolvin et al.[96] computed the structure of UO_4^{2-} to be tetrahedral, with a U−O distance of 1.90 Å. The closest analogy with the lowest energy structure of UO_4^- would seem to be that of WO_4^- as computed by Zhai et al.,[97] and later by Chen and Yang;[98] they found that WO_4^-, like UO_4^-, is a tetrakis-oxo species with a distortion from tetrahedral symmetry albeit much less of a distortion than for UO_4^- (Figure 1). The apparent similarity between UO_4^- and WO_4^- is notable as the highest oxidation states normally encountered in condensed phase chemistry are U(VI) and W(VI).

The computed geometrical parameters for UO_2, UO_2^+, UO_2^-, and UO_2^{2+} (Supporting Information, Table S1), each of which is linear, are in good agreement with those computed by others.[99−101] The structure of UO_3^- can be described as derived from UO_2^-, with a slight elongation of the O−U−O "uranyl" moiety, and a deviation from linearity by ~20°; the third uranium−oxygen bond is only slightly longer than the two equivalent "uranyl" bonds. In contrast to low-symmetry UO_3^-, the structure of WO_3^- is C_{3v};[97] the retention of the distorted "uranyl" moiety appears to dominate the structures of the uranate ions. The structure of UO_4H^-, which is the hydroxo species $UO_3(OH)^-$, corresponds to the addition of a hydroxo group to UO_3^-, with essentially no change in the O−U−O "uranyl" bond length or angle (Figure 1). As in the case of WO_3^- versus UO_3^-, the structure of $WO_3(OH)^-$[102] is much more symmetrical than that of $UO_3(OH)^-$. The previously computed structures for $U(OH)_2$, $U(OH)_4$, $UO_2(OH)$, and $UO_2(OH)_2$[103] exhibit a close analogy with those computed here: for the two dioxo hydroxo species the "uranyl" moiety remains nearly linear, whereas in the bis- and tetra-hydroxo species there is no such propensity for a linear HO−U−OH structure.

(b). Secondary and Tertiary Product Ions. The geometrical parameters for the lowest-energy isomer of each of the seven product ions are shown in Supporting Information, Figure S4. In each of the products, as in the primary uranate reactant ions, the essential character of the O−U−O "uranyl"-like moiety as evident in the bare UO_2^- ion is retained, with only a slight elongation of the U−O bonds and some distortion from linearity. In the notable case of the tris-methoxide, $UO_5C_3H_9^-$ (**10^i**), the UO_2 unit is essentially unaltered from bare UO_2^-; the shown lowest energy structure with all of the methoxo groups below the equatorial plane is only a few kcal mol^{-1} lower in energy than the configuration with one of the three above that plane.

The distinctive character of the quasi-linear uranyl moiety in the species examined here is underlined by comparison with computed structures for $MO_3(OH)^-$, $MO_3(OCH_3)^-$, $MO_2(OH)_2^-$, and $MO_2(OH)(OCH_3)^-$ for M = Cr, Mo, W).[102] For these group VI transition metal species, no such propensity for a linear O=M=O unit is exhibited.

(92) Groenewold, G. S.; Cossel, K. C.; Gresham, G. L.; Gianotto, A. K.; Appelhans, A. D.; Olson, J. E.; Van Stipdonk, M. J.; Chien, W. *J. Am. Chem. Soc*. **2006**, *128*, 3075–3084.
(93) Bryantsev, V. S.; de Jong, W. A.; Cossel, K. C.; Diallo, M. S.; Goddard, W. A.; Groenewold, G. S.; Chien, W.; Van Stipdonk, M. J. *J. Phys. Chem. A* **2008**, *112*, 5777–5780.
(94) Leavitt, C. M.; Bryantsev, V. S.; de Jong, W. A.; Diallo, M. S.; Goddard, W. A.; Groenewold, G. S.; Van Stipdonk, M. J. *J. Phys. Chem. A* **2009**, *113*, 2350–2358.
(95) Aubriet, F.; Gaumet, J. J.; de Jong, W. A.; Groenewold, G. S.; Gianotto, A. K.; McIlwain, M. E.; Van Stipdonk, M. J.; Leavitt, C. M. *J. Phys. Chem. A* **2009**, *113*, 6239–6252.
(96) Bolvin, H.; Wahlgren, U.; Gropen, O.; Marsden, C. *J. Phys. Chem. A* **2001**, *105*, 10570–10576.
(97) Zhai, H.-J.; Kiran, B.; Cui, L.-F.; Li, X.; Dixon, D. A.; Wang, L.-S. *J. Am. Chem. Soc*. **2004**, *126*, 16134–16141.
(98) Chen, Z. Y.; Yang, J. L. *Chin. J. Chem. Phys*. **2007**, *20*, 78–82.
(99) Zhou, M. F.; Andrews, L.; Ismail, N.; Marsden, C. *J. Phys. Chem. A* **2000**, *104*, 5495–5502.
(100) Ruipérez, F.; Danilo, C.; Réal, F.; Flament, J. P.; Vallet, V.; Wahlgren, U. *J. Phys. Chem. A* **2009**, *113*, 1420–1428.
(101) Réal, F.; Vallet, V.; Marian, C.; Wahlgren, U. *J. Chem. Phys*. **2007**, *127*, 214302–214311.
(102) Waters, T.; Wang, X. B.; Li, S. G.; Kiran, B.; Dixon, D. A.; Wang, L. S. *J. Phys. Chem. A* **2005**, *109*, 11771–11780.
(103) Wang, X. F.; Andrews, L. *Inorg. Chem*. **2006**, *45*, 4157–4166.

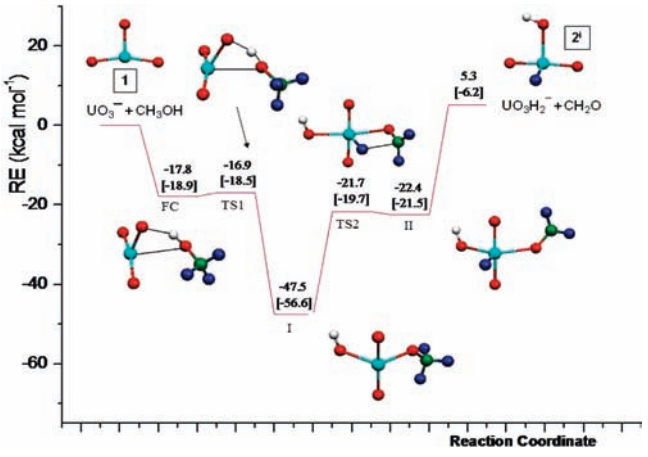

Figure 2. PEP for the reaction ***A*** of UO_3^- + CH_3OH (doublet spin state) at PW91/ZORA [B3LYP/SDD] level of theory. The labeling between the reactants and products identifies the first association complex (FC), the transition states (**TS1** and **TS2**), and the intermediates (**I** and **II**).

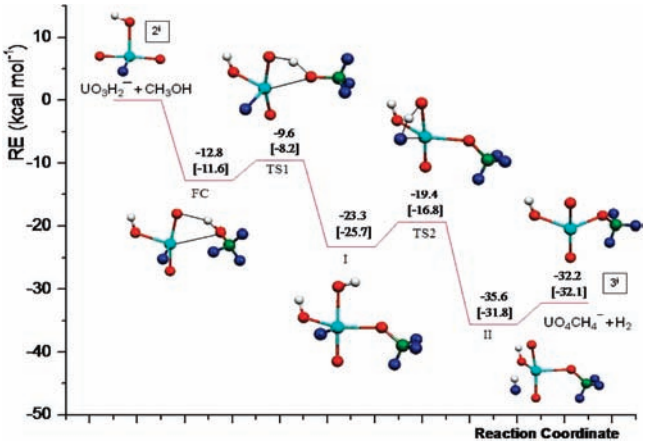

Figure 3. PEP for the reaction ***B*** of $UO_3H_2^-$ + CH_3OH (doublet spin state) at PW91/ZORA [B3LYP/SDD] level of theory.

(c). Oxidation States. Referring to the computed structures of the reactants and products, formal oxidation states at the uranium metal center can reasonably be assigned, with the notable exception of UO_4^-, for which the *formal* oxidation state of U(VII) is not credible. Throughout reaction sequence 1, the oxidation state U(V) is retained for the reactants and products. Similarly, throughout sequence 3, the oxidation state U(VI) is retained. After the anomalous UO_4^- reactant ion is converted to pentavalent $UO_2(OH)_2^-$ in reaction sequence 2, the oxidation state U(V) is subsequently retained.

Computed Reaction Pathways and Energetics. The computed PEP for each of the eight reactions, ***A***−***H***, in Scheme 1 is shown in Figures 2−9; the geometrical parameters for all of the intermediates and transition states, as well as the TS imaginary frequencies, are given in the Supporting Information, Figures S5−S12. To facilitate comparison of the computations with the isotopic labeling experiments, the color coding in Figures 2−9 and Supporting Information, Figures S5−S12 distinguishes the distribution of the protons (white) from the deuterons (blue) as is predicted from the mechanisms specifically for the reactions

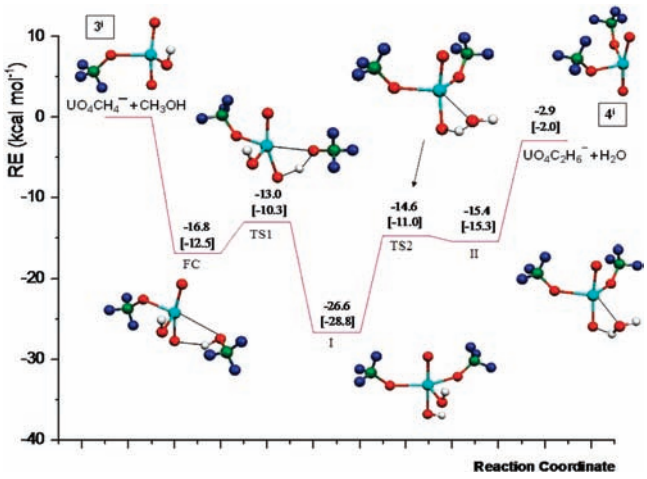

Figure 4. PEP for the reaction ***C*** of $UO_4CH_4^-$ + CH_3OH (doublet spin state) at PW91/ZORA [B3LYP/SDD] level of theory.

with CD_3OH discussed below; however, all of the computed parameters are for the fully protonated species.

For each of the eight reactions, the first transition state corresponds to the transfer of the methanolic proton to a uranium oxo ligand, which produces the first intermediate **I**, in which an oxo ligand has been converted to a hydroxo ligand and the resulting methoxo ligand is bound to the uranium metal center. This is in close analogy with the pathways computed for the reactions of MO^+ (M = V, Nb, Ta) with methanol, in which H_2 is eliminated to produce $MO_2CH_2^+$.[70] With the exception of reaction ***H***, this first intermediate is stable by at least 20 kcal mol^{-1} relative to the reactants. The mechanisms as they proceed from the intermediate **I** are discussed as classified by the neutral eliminated species; these elimination processes generally proceed by similar pathways.

(a). Elimination of Formaldehyde (Reactions *A* and *D*).

$$(A) \qquad UO_3^- + CH_3OH \rightarrow HUO_2(OH)^- + CH_2O \quad (1)$$

$$(D) \qquad UO_4^- + CH_3OH \rightarrow UO_2(OH)_2^- + CH_2O \quad (2)$$

The PEPs for reactions ***A*** (Figure 2) and ***D*** (Figure 5) are similar to one another up to the formation of the first intermediates, $UO_2(OH)(OCH_3)^-$ and $UO_3(OH)(OCH_3)^-$, respectively, which are formed by the mechanism common to all of the reactions, as described above. In the case of ***A***, the methyl hydrogen then transfers to the uranium metal center via **TS2** to the shallow intermediate **II**, $HUO_2(OH)(OCH_2)^-$, from which OCH_2 is eliminated. In the case of ***D***, the methyl hydrogen is transferred to an oxo-ligand to give the stable intermediate **II**, $UO_2(OH)_2(OCH_2)^-$, from which OCH_2 is eliminated.

Two alternative PEPs, Paths 2 and 3, for the reaction of UO_3^- with CH_3OH are shown in the Supporting Information, Figure S13, along with the confirmed favorable Path 1, which is shown in Figure 2. Path 2 gives the same product as Path 1, but the energetics of Path 2 are unfavorable. Path 3 leads to the energetically unfavorable high-energy bis-hydroxide product $UO(OH)_2^-$. The intriguing hydride hydroxide product **2** from reaction ***A***, as

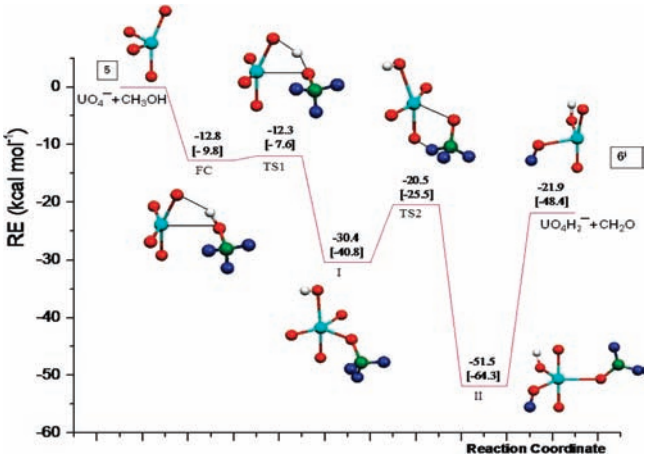

Figure 5. PEP for the reaction ***D*** of UO_4^- + CH_3OH (doublet spin state) at PW91/ZORA [B3LYP/SDD] level of theory.

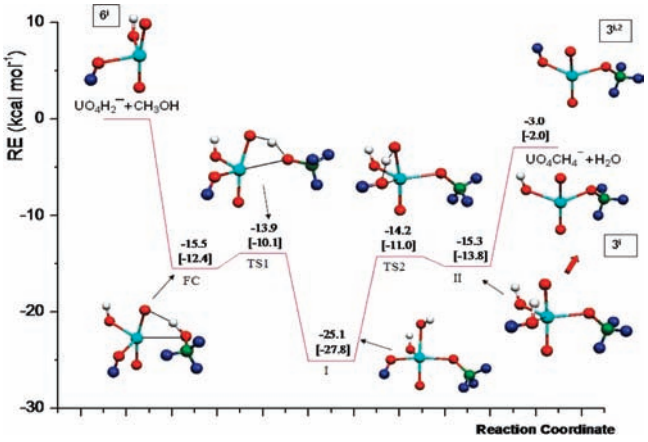

Figure 6. PEP for the reaction ***E*** of $UO_4H_2^-$ + CH_3OH (doublet spin state) at PW91/ZORA [B3LYP/SDD] level of theory.

well as the computed mechanism leading to it (i.e., Path 1), were confirmed by isotopic labeling studies described below.

In direct analogy with reaction ***A***, the reaction of NbO_3^- with methanol was similarly found to result in a product with the composition $NbO_3H_2^-$,[66] which was initially presumed to be the bis-hydroxo ion, Nb(III)O-$(OH)_2^-$. Subsequently, the reaction of VO_3^- with methanol was studied, along with a theoretical examination of both the VO_3^-/CH_3OH and the NbO_3^-/CH_3OH reaction pathways.[73] For both reactions the first intermediate is the $MO_2(OH)(OCH_3)^-$ ion, as for UO_3^-. The $VO_2(OH)$-$(OCH_3)^-$ ion primarily eliminates water to produce $VO_2(\eta^2$-$OCH_2)^-$. In contrast, $NbO_2(OH)(OCH_3)^-$ primarily eliminates formaldehyde to produce what was computed to be the hydride hydroxide, $HNbO_2(OH)^-$, via proton transfer from the methyl group to the Nb metal center;[73] this is essentially the same mechanism as found for the UO_3^-/CH_3OH reaction (Figure 2). Notably, other MO_3^- ions (M = Mn, Fe, Co) have been found to be inert toward methanol.[65]

In reaction ***D*** (Figure 5), a methyl hydrogen transfers to an oxo-ligand rather than to the uranium metal center to form the intermediate **II**, $UO_2(OH)_2(\eta^1$-$OCH_2)^-$ from which CH_2O is eliminated. The stability of the intermediate **II** and resulting barrier to formaldehyde elimination may relate to the relatively slow kinetics for this reaction. The η^1-OCH_2 structure of intermediate **II** here contrasts with the η^2 coordination in the product of the following reaction of VO_3^-: $VO_3^- + CH_3OH \rightarrow VO_2(\eta^2$-$OCH_2)^- + H_2O$, which proceeds very efficiently.[73]

(b). Elimination of Dihydrogen (Reaction *B*).

$$(\boldsymbol{B}) \qquad HUO_3(OH)^- + CH_3OH \rightarrow UO_2(OH)(OCH_3)^- + H_2 \qquad (3)$$

For reaction ***B*** (Figure 3), intermediate **I** eliminates H_2 by the combination of the hydridic proton with a hydroxo proton. The computed mechanism indicates that the hydroxo proton comes from the axial hydroxo group in intermediate **I**, not the equatorial hydroxo group; this particular aspect of the mechanism was experimentally confirmed as discussed below.

(c). Elimination of Water (Reactions *C*, *E*, *F*, and *H*).

$$(\boldsymbol{C}) \qquad UO_2(OH)(OCH_3)^- + CH_3OH \rightarrow UO_2(OCH_3)_2^- + H_2O \qquad (4)$$

$$(\boldsymbol{E}) \qquad UO_2(OH)_2^- + CH_3OH \rightarrow UO_2(OH)(OCH_3)^- + H_2O \qquad (5)$$

$$(\boldsymbol{F}) \qquad UO_3(OH)^- + CH_3OH \rightarrow UO_3(OCH_3)^- + H_2O \qquad (6)$$

$$(\boldsymbol{H}) \qquad UO_2(OH)(OCH_3)_2^- + CH_3OH \rightarrow UO_2(OCH_3)_3^- + H_2O \qquad (7)$$

Each of the reactions ***C*** (Figure 4), ***E*** (Figure 6), ***F*** (Figure 7), and ***H*** (Figure 9) correspond to replacement of a hydroxo ligand with a methoxo ligand with concomitant loss of water, and all exhibit similar mechanisms. The first intermediates, produced as described above, comprise two hydroxo ligands. In each case, a proton from one of these hydroxo ligands is transferred to the second hydroxo ligand to produce a second intermediate **II** which incorporates a H−O−H ligand; these second intermediates lie ∼11−15 kcal mol^{-1} below the reactant energies. Although the geometrical parameters for the four intermediates **II** are somewhat different, as shown in the Supporting Information, Figures S7, S9, S10, and S12, their binding energies are rather similar and elimination of H_2O requires only ∼9−12 kcal mol^{-1}; this water binding energy is only about a quarter of the binding energy of water to uranyl, UO_2^{2+}, in the gas phase.[42]

(d). Addition of Methanol (Reaction *G*).

$$(\boldsymbol{G}) \quad UO_3(OCH_3)^- + CH_3OH \rightarrow UO_2(OH)(OCH_3)_2^- \qquad (8)$$

The mechanism for the addition reaction ***G*** (Figure 8) is analogous to the process leading to the first intermediate for all of the other reactions. However, for reaction ***G***, the species corresponding to "intermediate **I**" for the other reactions is not an intermediate, but is instead the product.

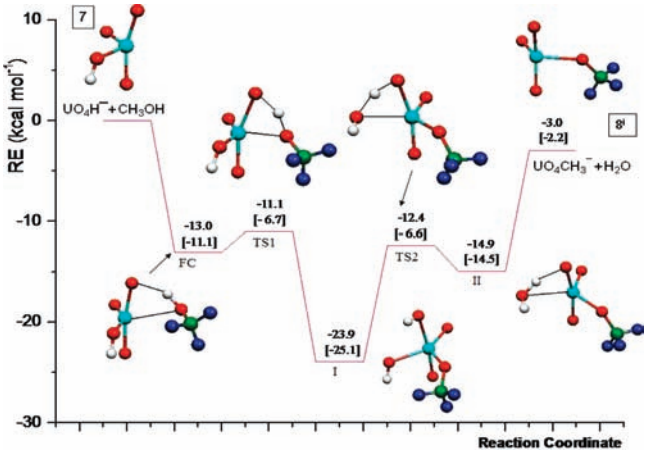

Figure 7. PEP for the reaction ***F*** of UO_4H^- + CH_3OH (singlet spin state) at PW91/ZORA [B3LYP/SDD] level of theory.

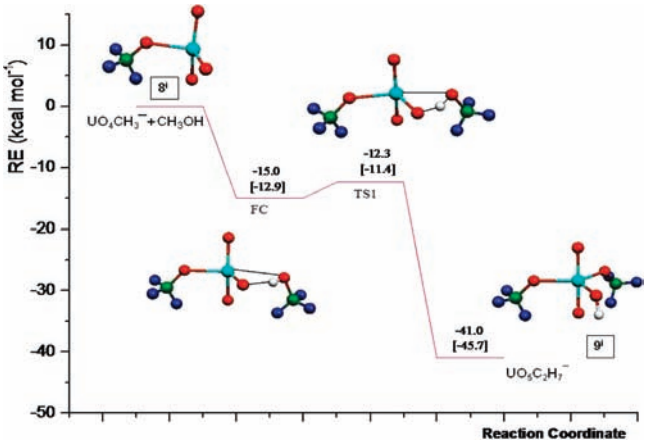

Figure 8. PEP for the reaction ***G*** of $UO_4CH_3^-$ + CH_3OH (singlet spin state) at PW91/ZORA [B3LYP/SDD] level of theory.

(e). Net Reaction Energetics: Bond Energies. In accord with IUPAC standards,[104] we interchangeably refer to bond dissociation energies and enthalpies. In reactions ***C***, ***E***, ***F***, and ***H***, a hydroxo group bound to the uranium metal center is replaced by a methoxo group, concomitant with elimination of H_2O. Accordingly, the net energetics for each of these reactions should be similar, as was computed. Each of these four reactions was found to be exoergic by ~3 kcal mol^{-1}, which suggests that the produced U−OCH_3 bonds are stronger than the broken U−OH bonds by ~11 kcal mol^{-1} (i.e., $\Delta H[CH_3OH + OH \rightarrow CH_3O + H_2O] = -14$ kcal mol^{-1} [105]). Reaction ***A*** is computed to be endoergic by 5 kcal mol^{-1} at the PW91/ZORA level and exoergic by 6 kcal mol^{-1} at the B3LYP/SDD level; assuming that the reaction is nearly thermoneutral, the reaction $UO_3^- + 2H \rightarrow HUO_2(OH)^-$ is exoergic by ~125 kcal mol^{-1} (i.e., $\Delta H[CH_3OH \rightarrow CH_2O + 2H] = 125$ kcal mol^{-1} [105]). The computed exoergicity of reaction ***B*** of 32 kcal mol^{-1} indicates that the U−OCH_3 bond in the product is ~33 kcal mol^{-1} stronger than the U−H bond in the reactant (i.e., $\Delta H[CH_3OH + H \rightarrow CH_3O + H_2] = 1$ kcal mol^{-1} [105]). This latter result is in qualitative accord with experimental results for highly oxophilic metal ions, such as Ti^+,[106] but the difference between the U−OH and U−H bond strengths is evidently somewhat smaller than in the case of Ti^+, perhaps suggesting greater covalency in the case of uranium. For reaction ***D***, the discrepancy between the computed net reaction energies at the two levels of theory is rather large, although both indicate a substantial exoergicity, of at least ~120 kcal mol^{-1} (based on the donation of two H atoms from CH_3OH as noted above), for the reaction $UO_4^- + 2H \rightarrow UO_2(OH)_2^-$. The computed energetics for reaction ***G*** indicate that $\Delta H[UO_3(OCH_3)^- + CH_3O + H \rightarrow UO_2(OCH_3)_2(OH)] \approx -150$ kcal mol^{-1}.

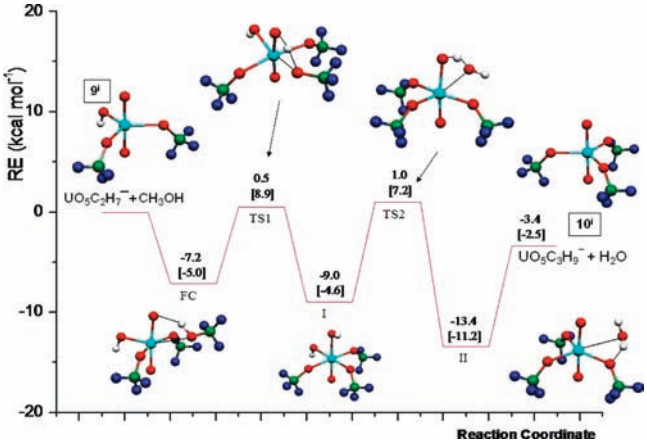

Figure 9. PEP for the reaction ***H*** of $UO_5C_2H_7^-$ + CH_3OH (singlet spin state) at PW91/ZORA [B3LYP/SDD] level of theory.

(f). Inert Nature of UO_2^-. In an attempt to understand the distinctively unreactive character of UO_2^-, the PEPs for the hypothetical reactions given by eqs 9−12 were computed.

$$UO_2^- + CH_3OH \rightarrow HUO_2(OCH_3)^- \quad (9)$$

$$UO_2^- + CH_3OH \rightarrow (HO)UO(OCH_3)^- \quad (10)$$

$$UO_2^- + CH_3OH \rightarrow UO_3^- + CH_4 \quad (11)$$

$$UO_2^- + CH_3OH \rightarrow UO_2(OH)^- + CH_3 \quad (12)$$

The reactions given by eqs 9 and 10 were computed only at the B3LYP/SDD level of theory because of problems characterizing the transition structures at the PW91/ZORA level; those given by 11 and 12 were computed at both the B3LYP/SDD and PW91/ZORA levels. The computed PEPs and geometrical parameters are given in the Supporting Information, Figures S14 and S15. The results indicate that 9, 10, and 11 are all substantially exoergic, by at least 30 kcal mol^{-1}, and that 12 is evidently only slightly exoergic. The observation that none of these reactions proceeds, even those which are highly energetically favorable, can be attributed to the first transition states, which lie very near to, or perhaps slightly above, the energy of the

(104) http://goldbook.iupac.org/index.html.
(105) *NIST, Chemistry WebBook, NIST Standard Reference Database Number 69*; Linstrom, P. J., Mallard, W. G., Eds.; National Institute of Standards and Technology: Gaithersburg, MD; http://webbook.nist.gov (accessed December 2, 2009).

(106) Armentrout, P. B.; Kiran, B. In *Organometallic Ion Chemistry*; Freiser, B. S., Ed.; Kluwer: Dordrecht, 1996; pp 1−45.

entrance channel. For 9, 11, and 12, these first transition states correspond to bonding between the methanolic oxygen and the uranium metal center, U···O−C. This contrasts with all of the observed reactions (Figures 2−9), where the first transition states are complexes with bonding between uranium and the methanolic oxygen, U···O−C, concomitant with bonding between the methanolic hydrogen and a uranium-oxo group, H···O−U. For the reaction given by eq 10, the rather distinctive first complex (see Supporting Information, Figure S14) proceeds to a transition state which invokes the typical U···O−C and H···O−U bonding interactions seen with the mechanisms for the observed reactions; however, this TS in this case lies close to the reactant entrance energy level and evidently presents a barrier to the reaction. A factor which may contribute to the relatively unreactive character of UO_2^- is that it has fewer degrees of freedom for dissipation of energy in the initial complex which can result in facile back reaction. As the initial ion-neutral complexes for the computed UO_2^-/methanol reactions (i.e., the FCs in Supporting Information, Figures S14 and S15) are less stable than the FCs for the UO_3^-, UO_4^-, or UO_4H^-, there is less energy for reactions to proceed which often leads to fast back reactions. Reactions ***B***, ***C***, ***D***, ***E***, ***F***, and ***H*** each progress through an intermediate **I** on their PEPs in which one of the axial "uranyl-like" oxo-ligands has become hydroxylated. From the results in Supporting Information, Table S1, it is apparent that the computed charges on the oxo-ligands in UO_2^- (−1.09) are intermediate between those on the "equatorial" oxo-ligands in UO_3^- (−1.26) and UO_4^- (−0.96); that the latter two ions do react whereas UO_2^- is inert is thus evidently not directly attibutable to the susceptibility of the oxo-ligands to initial electrophilic attack. The origin of the relatively high-energy FCs, and first transition states, for UO_2^- (i.e., FC and FC′ in Supporting Information, Figure S14 and FC in Supporting Information, Figure S15) is instead likely related to the relatively low charge on the uranium metal center. In UO_2^- the computed uranium charge is 1.18 whereas in UO_3^- it is 2.65 and in UO_4^- it is 2.79 (Supporting Information, Table S1). The distinctive character of FC′, in which the methanolic hydrogen coordinates to an oxo-ligand without any interaction between the methanolic oxygen and uranium, is likely a manifestation of the much lower uranium charge in UO_2^-. It should be noted that in contrast to inert UO_2^-, CoO_2^- readily reacts with methanol,[65,107] to produce what is postulated as $Co(OH)_2^-$ ($+CH_2O$);[107] other MO_2^- (M = Mn, Fe, Ni, Cu) also react with methanol to produce the $MO_2H_2^-$ ions.[65]

Observed Reactions with Methanol Isotopologues. The labeled methanol molecules were used to track the distribution of the reactant atomic constituents in the products. For several reactions, comparison of the observed isotopic distributions with those predicted by the details of the computed PEPs provided clear experimental confirmation of the theoretical results. It was thus possible to essentially confirm the computed mechanisms without directly examining the dynamics of the reactions. These labeling studies additionally confirmed some of the computed structures, including that of $UO_3H_2^-$ as a hydride hydroxide.

(a). CD_3OH and CD_3OH/CD_3OD Mixture. The three reaction sequences were studied in detail for CD_3OH as these reactions provided particularly useful insights into mechanisms, especially for reactions ***A***, ***B***, and ***E***. The reaction sequences for CD_3OH are summarized in Scheme 2, using nomenclature analogous to that in Scheme 1 for CH_3OH but with a distinguishing superscript "i"; for reaction $\boldsymbol{E^i}$, there are two isotopic channels, designated as $\boldsymbol{E^{i,1}}$ and $\boldsymbol{E^{i,2}}$. The reaction efficiencies, k/k_{COL}, are included in Scheme 2 in italics; the absolute pseudo-first order rate constants are obtained by multiplying these k/k_{COL} values by $k_{COL} \approx 1.7 \times 10^{-9}$ cm^3 molecule^{-1} s^{-1}, which varies by only 4% among these reactions. It is notable that there was no detectable isotopic scrambling, with the exception of reaction $\boldsymbol{E^i}$ where two isotopic channels are expected from the mechanism, as discussed below. The apparently complete retention of isotopic labeling is in accord with the purported thermal nature of these bimolecular reactions. Although all of the computations were performed for the fully protonated species, to facilitate comparison of the experimental results for CD_3OH with the computed reaction pathways, Figures 2−9 show deuterium atoms in blue and protons in white.

i. Reactions *A* and *B*. The computed lowest energy path for reaction ***A*** indicates that the product is a hydroxide hydride rather than a bis-hydroxide, with the latter isomer computed to be ~30 kcal mol^{-1} higher in energy (Supporting Information, Figure S13). As seen in Figure 2, it is predicted from the PEP that product $\mathbf{2^i}$, UO_3HD^-, is the hydroxide deuteride, $DUO_2(OH)^-$, not the deuteroxide hydride, $HUO_2(OD)^-$. The observation of exclusively HD-elimination for reaction $\boldsymbol{B^i}$, corresponding to product $\mathbf{3^i}$ in Figure 3, provides convincing confirmation of the computed structure for **2**, as well as for the computed mechanisms for ***A*** and ***B***. For reaction $\boldsymbol{B^i}$, exclusive HD-loss, absent H_2-loss, indicates that the H and D atoms in $\mathbf{2^i}$ are not equivalent, as in the proposed hydroxide deuteride structure. More specifically, exclusive loss of HD from $\mathbf{2^i}$ is indicative of a deuteride hydroxide, and the proposed mechanism for $\boldsymbol{B^i}$ (Figure 3); if $\mathbf{2^i}$ were instead a hydride deuteroxide then only H_2-elimination would occur. If $\mathbf{2^i}$ were a mixture of $HUO_2(OD)^-$ and $DUO_2(OH)^-$ then both H_2- and HD-elimination would occur. The experimental observation of solely HD-elimination thus corroborates the computed structure of **2**, as well as the computed paths for reactions ***A*** and ***B***.

The structure of **2** and the dehydrogenation mechanism for ***B*** were further confirmed using the roughly equimolar mixture of CD_3OH and CD_3OD. The reaction of $DUO_2(OH)^-$, $\mathbf{2^i}$, with this mixture produced exclusively $UO_4CD_3H^-$ (i.e., $UO_2(OH)(OCD_3)^-$); the absence of any fully deuterated product from the CD_3OD component of the reactant mixture indicates that the equatorial OH group in intermediate **I** remains in the product, as well as that deuteride ligand is eliminated, in accord with TS2. The reaction of $DUO_2(OD)^-$ with the CD_3OH/CD_3OD mixture produced exclusively $UO_4CD_4^-$ (i.e., $UO_2(OD)(OCD_3)^-$); the absence of any monoprotonated product from the CD_3OH component indicates that the equatorial OD group

(107) Yi, M. N.; Fisher, K. J.; Dance, I. G. *Int. J. Mass Spectrom.* **2002**, *216*, 155–168.

Scheme 2[a]

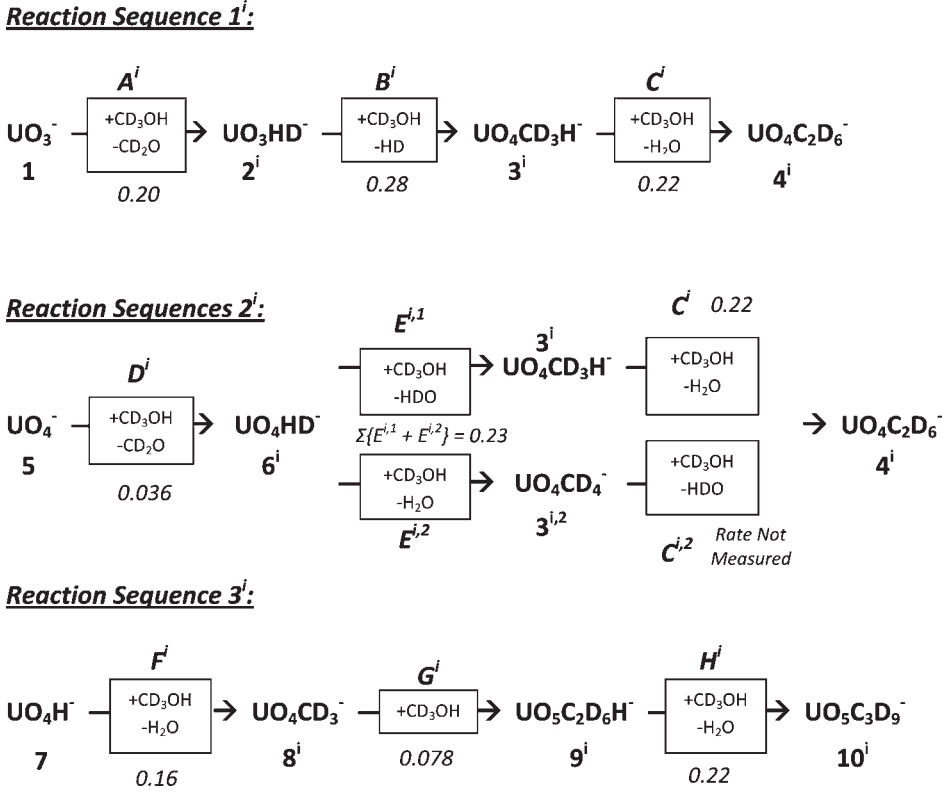

[a] k/k_{COL} values are given in italics.

in intermediate **I** remains in the product, again in clear accord with TS2. These results provide corroboration of the structure of **2**, and the details of the computed reaction mechanism for ***B***, including quite specifically that hydrogen elimination proceeds through the intermediate **I** and interaction of the axial hydroxo group and the hydride ligand as indicated by TS2.

Two alternative PEPs for the reaction between UO_3^- and CH_3OH were computed; these Paths 2 and 3, are shown in the Supporting Information, Figure S13. The identification of the product of the UO_3^-/CD_3OH reaction as $DUO_2(OH)^-$ confirms the conclusion that Path 1, the favorable computed path, is the actual path. Because the U−H moiety in the product of Path 2, which also leads to the hydride hydroxide product, comes from the methanolic group rather than the methyl group, the product would be $HUO_2(OD)^-$ rather than the observed $DUO_2(OH)^-$. The product of Path 3, which is energetically quite unfavorable, would be the bis-hydroxide, $UO(OH)(OD)^-$ and would exhibit isotopic scrambling in the subsequent dihydrogen elimination.

This convincing corroboration of the computed PEPs for reactions ***A*** and ***B*** provides confidence in the validity of the computational methodologies to reliably provide reaction mechanisms for the types of reactions studied here.

ii. Reaction *E*. The simultaneous occurrence of reactions $E^{i,1}$ (i.e., HDO-elimination from UO_4HD^-) and $E^{1,2}$ (i.e., H_2O-elimination from UO_4HD^-) is in accord with the proposed bis-hydroxide structure of **6**. If the H and D atoms in $\mathbf{6}^{\mathbf{i}}$ were not equivalent, as in a deuteride hydroxide, for example, isotopic specificity such as that for UO_3HD in reaction B^i would be expected. A feasible alternative to the computed pathway for reaction ***E*** would be a "concerted" mechanism in which water elimination occurs by the intermediate **I**, followed by an interaction between the two equatorial hydroxo ligands of the reactant ion. However, as only HDO-elimination would result from such a concerted mechanism, the observed H_2O-elimination pathway $E^{i,2}$ apparently refutes this possibility.

From the computed mechanism, it is expected that the reaction of UO_4HD^- with CD_3OH, that is, concurrent reactions $\{E^{i,1}$ & $E^{i,2}\}$, should produce roughly comparable yields of $UO_4CD_3H^-$ (i.e., $\mathbf{3}^{\mathbf{i}}$ via $\mathbf{E}^{\mathbf{i,1}}$) and $UO_4CD_4^-$ (i.e., $\mathbf{3}^{\mathbf{i,2}}$ via $\mathbf{E}^{\mathbf{i,2}}$); this evaluation does not consider a skewed distribution due to a kinetic isotope effect. Because of the slow kinetics for D^i it is problematic to quantitatively study $E^{i,1}$ and $E^{i,2}$; as indicted in Scheme 2, only the overall kinetics for $\{E^{i,1}$ & $E^{i,2}\}$ were determined, not the individual contributions. Under these reaction conditions, it was demonstrated that concurrent reactions $\{E^{i,1}$ & $E^{i,2}\}$ produced more $UO_4CD_3H^-$ than $UO_4CD_4^-$. The observation that HDO-elimination from intermediate **I** (i.e., reaction $E^{i,1}$) dominates over H_2O-elimination (i.e., reaction $E^{i,2}$) could suggest that the proton in the axial hydroxo ligand in intermediate **I** is not necessarily eliminated, as indicated in TS2, but instead that water-elimination may also proceed via interaction between the equatorial OH and OD ligands in intermediate **I**. However, the inability to effectively thermalize $\mathbf{6}^{\mathbf{i}}$ because of the particular kinetics of this sequence precludes such a definitive interpretation.

The mechanism for reaction ***E*** was further examined by reacting $UO_4D_2^-$ with the CD_3OH/ CD_3OD mixture. The result was a substantial excess of $UO_4CD_4^-$, and a lesser yield of $UO_4CD_3H^-$, in an approximate ratio of 4:1. An alternative "concerted" mechanism, as described above, would have resulted in exclusively D_2O elimination and comparable yields of $UO_4CD_4^-$ and $UO_4CD_3H^-$. If the mechanism proceeds through intermediate **I** and TS2, the sole product would have been $UO_4CD_4^-$ because one of the two eliminated hydrogens comes from the axial hydroxo. The observation of a small yield of $UO_4CD_3H^-$ is consistent with intermediate **I**, but not necessarily exclusive involvement of the axial hydroxo in the subsequent water elimination, as formally indicated by TS2.

In summary, the experimental results suggest that the computed mechanism for reaction E^i is valid, except that the proton transfer in **TS2** may alternatively involve the two equatorial hydroxo groups in intermediate **I**, and not necessarily exclusively the axial hydroxo group. However, it should be emphasized that the experimental results are not definitive because of the inability to effectively thermalize the reactant ion $\mathbf{6}^i$. The potentially hyperthermal experimental results do not necessarily refute the computed mechanism. The key conclusion is that the structure of $\mathbf{6}^i$ is valid, and the mechanism does proceed through the tris-hydroxy intermediate **I**.

iii. Reactions *C*, *D*, *F*, *G*, and *H*. Reactions ***C***, ***F***, and ***H*** each proceed by the reaction of a monohydroxilated ion with CH_3OH and elimination of H_2O. According to the computed mechanisms, one of the two eliminated H atoms derives from the methanolic group and the other from the hydroxo group. In accord with these mechanisms, for reactions C^i, F^i, and H^i only H_2O is eliminated. Specifically, the D-atoms in the CD_3OH reactant molecule and, for C^i and H^i, the deuterated methoxo groups in the reactant ion, remain in the product. The CD_3 groups remain intact, as predicted from the computed mechanisms.

The results for reaction D^i, exclusive elimination of CD_2O, confirm that one of the two hydrogen atoms in the product ion comes from the methyl group and the other from the methanolic group. This is again in accord with the computed mechanism.

As reaction ***G*** is addition of an entire methanol molecule to the reactant ion, the isotopic labeling experiments are informative only in the context of the kinetic isotope effect, as discussed below.

iv. Summary for CD_3OH and CD_3OD. The mechanistic insights gleaned from the result using the CD_3OH and CD_3OD isotopologues can be summarized as follows: (1) The structure of $\mathbf{2}^i$ and thereby indirectly the PEP for ***A*** were confirmed. (2) PEP ***B*** was confirmed. (3) PEP ***E*** was validated, except that the exclusive involvement of the axial OH-group in **TS2** could not be definitively confirmed. (4) The results are entirely consistent with the PEPs for ***C***, ***D***, ***F***, and ***H***, although the mechanistic details could not be conclusively verified.

(b). $CH_3{}^{18}OH$. Using the O-18 substituted methanol isotopologue, $CH_3{}^{18}OH$, it was found that ^{18}O was incorporated into the anion product for reactions ***B***, ***C***, ***E***, ***F***, ***G***, and ***H***, but not for ***A*** or ***D***. As with deuterated methanol, these reactions were isotopically pure, with no detectable isotopic mixing. Referring to the reaction and product labeling in Scheme 1, the corresponding observed products for $CH_3{}^{18}OH$ are as follows, where the reactions and products are identified with daggers. The product ions which contained ^{18}O are as follows: $UO_3{}^{18}OCH_4^-$ ($\mathbf{3}^\dagger$ from $B^\dagger$ and $E^\dagger$); $UO_2{}^{18}O_2C_2H_6^-$ ($\mathbf{4}^\dagger$ from $C^\dagger$); $UO_3{}^{18}OCH_3^-$ ($\mathbf{8}^\dagger$ from $F^\dagger$); $UO_3{}^{18}O_2C_2H_7^-$ ($\mathbf{9}^\dagger$ from $G^\dagger$); and $UO_2{}^{18}O_3C_3H_9^-$ ($\mathbf{10}^\dagger$ from $H^\dagger$). These reactions, with the isotopic structures as predicted from the computed PEPs, are given in eqs 13−20, where the unlabeled O-atoms are ^{16}O.

$$A^\dagger \quad UO_3^- + CH_3{}^{18}OH \rightarrow HUO_2(OH)^- + CH_2{}^{18}O \quad (13)$$

$$B^\dagger \quad HUO_2(OH)^- + CH_3{}^{18}OH \rightarrow UO_2H(^{18}OCH_3)^- + H_2 \quad (14)$$

$$C^\dagger \quad UO_2H(^{18}OCH_3)^- + CH_3{}^{18}OH \rightarrow UO_2(^{18}OCH_3)_2^- + H_2O \quad (15)$$

$$D^\dagger \quad UO_4^- + CH_3{}^{18}OH \rightarrow UO_2(OH)_2^- + CH_2{}^{18}O \quad (16)$$

$$E^\dagger \quad UO_2(OH)_2^- + CH_3{}^{18}OH \rightarrow UO_2(OH)(^{18}OCH_3)^- + H_2O \quad (17)$$

$$F^\dagger \quad UO_3(OH)^- + CH_3{}^{18}OH \rightarrow UO_3(^{18}OCH_3)^- + H_2O \quad (18)$$

$$G^\dagger \quad UO_3(^{18}OCH_3)^- + CH_3{}^{18}OH \rightarrow UO_2(OH)(^{18}OCH_3)_2^- \quad (19)$$

$$H^\dagger \quad UO_2(OH)(^{18}OCH_3)_2^- + CH_3{}^{18}OH \rightarrow UO_2(^{18}OCH_3)_3^- + H_2O \quad (20)$$

The results for $B^\dagger$ and $G^\dagger$ are uninformative as no oxygen is eliminated in these reactions; the results for all of the other reactions are as predicted from the computed PEPs. The results are consistent with the proposed mechanisms for reactions $A^\dagger$ and $D^\dagger$ as the oxygen atom from the $CH_3{}^{18}OH$ reactant is eliminated in the formaldehyde product, $CH_2{}^{18}O$. The results for reactions $C^\dagger$, $E^\dagger$, $F^\dagger$, and $H^\dagger$, where the ^{18}O from $CH_3{}^{18}OH$ is incorporated into the products, confirm that the $^{18}OCH_3$ group remains intact, as is predicted from the computed mechanisms.

Reaction Kinetics. As is evident from the results in Table 1, six of the eight reactions with CH_3OH are rather facile and exhibit similar efficiencies, about 20% of the collisional rate. Reactions ***D*** and ***G*** are significantly less

efficient. It is not necessarily evident that the computed PEPs predict these comparative reaction efficiencies. To quantitatively predict/understand kinetics for such bimolecular reactions as studied here, it is necessary to perform dynamic calculations[108] rather than the stationary DFT computations performed in this work. It is nonetheless of interest to consider the observed kinetics in the context of the computed reaction pathways and possible rate-limiting steps. It should be noted that none of the computed reaction pathways involve a spin change, which would generally diminish reaction efficiencies, though not necessarily as much for reactions of many-electron actinides as for lighter transition metals.

In Supporting Information, Table S2 we summarize the computed energetics for the reactions at the two levels of theory. Also included there are the highest energy barriers on the computed PEP for each reaction. The results summarized in Supporting Information, Table S2 indicate reasonably good agreement between the two levels of theory, to within about 10 kcal mol^{-1}, with the conspicuous exception of reaction ***D*** where the net energies for the reaction are −22 and −42 kcal mol^{-1} at the PW91/ZORA and B3LYP/SDD levels of theory, respectively. The computed PEP barriers are also disparate for this reaction, which proceeds relatively inefficiently. It should be noted that reaction ***D*** is the only observed reaction in which there is a change in the formal oxidation state at the uranium metal center, from the anomalous tetrakis-oxo UO_4^- ion to $U^VO_2(OH)_2^-$. Previous theoretical studies have shown that DFT is prone to provide less accurate reaction energies when such changes in oxidation state occur.[50,109]

As remarked above, the computed similar net reaction energetics for ***C***, ***E***, ***F***, and ***H*** reflect the close correspondence between these four reactions, that is, replacement of an OH group by an OCH_3 group. Notably, the kinetics for these four reactions are essentially the same to within the experimental uncertainty: $0.17 \leq k/k_{COL} \leq 0.22$. For ***C***, ***E***, and ***F***, the computed mechanisms, that is, the structures and energetics along the potential energy surfaces, are quite similar such that similar kinetics would be expected. However, the computed mechanism for ***H*** is quite disparate; in particular, both **TS1** and **TS2** are seemingly rather awkward species which lie near, or slightly above, the reactant energies. From the static DFT results it appears somewhat remarkable that reaction ***H*** should proceed with the observed high efficiency. Given the linearity of the first-order kinetics data for this reaction it appears unlikely that the high efficiency is attributable to an excited state species; the lifetime of such an excited state would need to be ∼1 s or longer to result in the observed linearity. Adduct formation under the low-pressure (< 10^{-6} Torr) conditions of the experiments is generally not observed because of the infrequency of third-body collisions which remove energy and stabilize the energetic product; ion-neutral complexes under these conditions are instead stabilized by emission of IR radiation. It should be remarked that the CID results discussed below cannot differentiate between a CH_3OH adduct, that is, the first complex (FC) in Figure 8, and the computed hydroxide methoxide product 9.

In summary, although it is feasible that the computed PEP for reaction ***H*** is erroneous, this is most likely an example where dynamic computations would further illuminate the observed kinetics.

The relatively slow kinetics for reaction ***G*** are particularly intriguing as the computed mechanism encounters only a very small (B3LYP/SDD) or no (PW91/ZORA) energy barrier along the PEP, and the reaction is substantially exothermic (see Supporting Information, Table S2). However, it is a typical observation that such association reactions are inefficient. In the case of adduct formation, $A^- + B \rightarrow A^-{\bullet}B$, the reaction energy in the nascent excited-state product, $\{A^-{\bullet}B\}^*$, can enable the reverse dissociation pathway, which is facile for a simple adduct: $\{A^-{\bullet}B\}^* \rightarrow A^- + B$. However, the computed structure of the stable product **9**, which is not a simple adduct, is such that it might be expected that rearrangement and dissociation back to the reactants could be inefficient. In assessing the observed reaction efficiencies in the context of the computed energetics, the role of entropy in bimolecular ion−molecule reactions has been discussed elsewhere[110,111] and merits consideration here. In particular, it is noted that ***G*** is the only observed reaction which results in a decrease in the net number of particles, with two coalescing into one. It is generally considered that it is the enthalpy, not the free energy, of bimolecular reactions under low-pressure conditions which is thermodynamically (and kinetically) pertinent. For reactions of the general type $A^- + BC \rightarrow AB^- + C$, with no net change in the number of particles, deviations from this approximation should be, and generally are found to be, minor. However, for association reactions, $A^- + BC \rightarrow ABC^-$, such as reaction ***G***, the decrease in the number of particles may introduce a thermodynamically unfavorable, and undefined as the temperature is undefined during the isolated interaction of two particles, entropic effect.[110] This effect, which would not be revealed in the computed PEP, might account for the diminished reaction efficiency.

Kinetic Isotope Effects (KIEs). The kinetics for the three primary uranate ions with the four methanol isotopologues were measured and are given in Table 2, as k/k_{COL}. The kinetics are essentially the same for CH_3OH, CD_3OH, and $CH_3{}^{18}OH$. However, it is apparent that there is a significant reduction in reaction efficiencies for each of the three uranate ions with CD_3OD. In comparing the results for reactions upon substitution of OD for OH in the reactant methanol, specifically the comparative kinetics for CD_3OD and CD_3OH, it is evident that the reaction rates are reduced for the former. The KIE due to the higher zero point energy (ZPE) of the OH group is considered to reflect a reduction in energy barriers, and faster kinetics, for processes in the mechanisms which involve cleavage of an O−H rather than an O−D bond. The KIE is most pronounced for reaction ***F*** (UO_4H^-), for which no reaction with CD_3OD could be detected, and somewhat less pronounced, but still significant, for reactions ***A*** (UO_3^-) and ***D*** (UO_4^-). Referring to the PEPs for reactions ***A*** and ***D*** in Figures 2 and 5, it is apparent that deuterium substitution in the methanolic group, that is, in CD_3OD, should diminish the efficiency of the hydrogen-transfer which occurs in **FC** → **TS1**; for these two reactions, the

(108) López, J. G.; Vayner, G.; Lourderaj, U.; Addepalli, S. V.; Kato, S.; Dejong, W. A.; Windus, T. L.; Hase, W. L. *J. Am. Chem. Soc.* **2007**, *129*, 9976–9985.
(109) Vallet, V.; Schimmelpfennig, B.; Maron, L.; Teichteil, C.; Leininger, T.; Gropen, O.; Grenthe, I.; Wahlgren, U. *Chem. Phys.* **1999**, *244*, 185–193.
(110) Irikura, K. K. *J. Am. Chem. Soc.* **1999**, *121*, 7689–7695.
(111) Innorta, G.; Torroni, S.; Maranzana, A.; Tonachini, G. *J. Organomet. Chem.* **2001**, *626*, 24–31.

Table 2. − Relative Kinetics for Primary Reactions of Uranates with Methanol Isotopologues[a]

	CH_3OH	CD_3OH	CD_3OD[b]	$CH_3{}^{18}OH$
UO_3^- (***A***)	0.21	0.20	0.04	0.22
UO_4^- (***D***)	0.039	0.036	0.01	0.034
UO_4H^- (***F***)	0.17	0.16	<0.01	0.16

[a] The relative kinetics are given as k/k_{COL}. Absolute rate constants, k, are obtained by multiplying these k/k_{COL} values by $k_{COL} = 1.7 \times 10^{-9}$ cm^3 $molecule^{-1}$ s^{-1}, which is nearly constant for these reactant uranate ions and methanol isotopologues of similar masses. The reactions are identified in parentheses as labeled in Scheme 1, and the corresponding computed PEPs are shown in Figures 2, 5, and 7. [b] These values were derived from the measured overall rate constants for pure CD_3OH and a ~50%/50% mixture of CD_3OD/CD_3OH. The uncertainties associated with these values are accordingly somewhat greater than for the others.

uranium hydroxo group in intermediate **I** is not directly involved in the subsequent transfer of the methyl hydrogen, which is followed by formaldehyde elimination. In contrast, from the computed mechanism for reaction ***F*** (Figure 7), the methanolic proton is transferred in **FC** → **TS1** and then again in **I** → **TS2**, and is ultimately eliminated in the neutral HDO product. The particularly large KIE with CD_3OD in the specific case of reaction ***F*** may result from the direct involvement of the methanolic hydrogen in each step of the reaction mechanism.

For the reactions of UO_3^- (***A***), UO_4^- (***D***), and UO_4CD_3 (***G***^{i}) it was possible to employ relative product yields from the CD_3OH/CD_3OD mixture to evaluate the comparative kinetics for these two methanol isotopologues. The pertinent reactions are specified in eqs 21a, 21b, 22a, 22b, 23a, and 23b, where the reactions with CD_3OH are designated as ***A***^{i}, ***D***^{i}, and ***G***^{i}, as in Scheme 1, and the corresponding reactions with CD_3OD are designated as ***A***‡, ***D***‡, and ***G***‡.

$$\boldsymbol{A}^{i} \quad UO_3^- + CD_3OH \rightarrow DUO_2(OH)^- + CD_2O \quad (21a)$$

$$\boldsymbol{A}^{‡} \quad UO_3^- + CD_3OD \rightarrow DUO_2(OD)^- + CD_2O \quad (21b)$$

$$\boldsymbol{D}^{i} \quad UO_4^- + CD_3OH \rightarrow UO(OH)(OD)^- + CD_2O \quad (22a)$$

$$\boldsymbol{D}^{‡} \quad UO_4^- + CD_3OD \rightarrow UO(OD)_2^- + CD_2O \quad (22b)$$

$$\boldsymbol{G}^{i} \quad UO_3(OCD_3)^- + CD_3OH \rightarrow UO_2(OCD_3)_2(OH)^- \quad (23a)$$

$$\boldsymbol{G}^{‡} \quad UO_3(OCD_3)^- + CD_3OD \rightarrow UO_2(OCD_3)_2(OD)^- \quad (23b)$$

Among the reactions studied, only for mechanisms ***A***, ***D***, and ***G*** is the methanolic proton retained in the product ion, as is necessary to differentiate the reaction products and thereby obtain relative kinetics from the product abundances using the CD_3OH/CD_3OD mixture. The relative product yields for the concurrent pairs of CD_3OH and CD_3OD reactions provide the ratio of the rate constants, $k[CD_3OH]/k[CD_3OD]$. The results indicate that for each of the three reactions the kinetics for CD_3OD is slower, by a factor of approximately 2−3. For UO_3^- and UO_4^-, these values are somewhat smaller than the factors of 4−5 derived from the rate constants in Table 2, but are qualitatively consistent. For reactions ***A*** and ***D***, the KIE is rationalized as discussed above. In the case of ***G***, the observed KIE suggests the hydrogen transfer step in Figure 8, **FC** → **TS1**, presents a significant barrier upon substitution of D for H in the methanolic group. As indicated in Schemes 1 and 2, the KIE for reaction ***G*** using CD_3OH instead of CH_3OH is negligible, as expected if the methanolic proton is key in the reaction pathway.

As is evident from the results in Table 2, the kinetics are nearly the same for CH_3OH and CD_3OH, with only a very small, if any, decrease in the rate constant for the partially deuterated isotopologue. The reactions of UO_3^- and UO_4^- require the transfer of a methyl hydrogen, corresponding to **I** → **TS2** in the PEPs, Figures 2 and 5. The observation that the rate constants are essentially the same for CH_3OH and CD_3OH suggests that transfer of the methyl hydrogen is not rate-determining.

In summary, the KIE results are somewhat qualitative, but clearly reveal significantly slower kinetics for CD_3OD versus CD_3OH in reactions ***A***, ***D***, ***F***, and ***G***. For each of these four reactions the computed mechanism involves transfer of the methanolic hydrogen atom, which should be more facile for a proton than a deuteron. The KIE is particularly pronounced for reaction ***F*** as compared with ***A***, ***D***, and ***G***, which may reflect the involvement of the methanolic proton along the entire PEP, rather than during only one step as for the other three reactions. The KIE results suggest that the rate-determining steps for these reactions are not necessarily those with the highest energy barriers. Even when transfer of a methyl hydrogen atom occurs via a high-energy barrier, substitution of deuterium for the methyl protons results in a negligible effect on the rate constant.

CID. Several of the product ions were subjected to CID. The main results are summarized in Table 3. Only the elementary dissociation channels are specified; loss of more than one neutral species was observed for some parent ions, but these multiple-elimination processes are generally less directly informative about the structure of the parent ion. The structures of the eliminated neutrals are assumed to be the stable molecules, dihydrogen, water, methanol, or formaldehyde. As discussed below, the isotopic compositions of the eliminated species are consistent with the postulated structures. In particular, the isotopic compositions of products from CID of the deuterium-labeled ions, **2**^{i}, **3**^{i}, **4**^{i}, **6**^{i}, **8**^{i}, **9**^{i}, and **10**^{i}, generally do not definitively elucidate their structures, but are entirely consistent with them.

The sole association product **9**^{i}, $UO_5C_2D_6H^-$ ion, cleanly dissociates into only $UO_4CD_3^-$ (+ CH_3OH). It is presumed that this product has the structure **8**^{i} and that the dissociation proceeds by the reverse of the mechanism for ***G***^{i} shown in Figure 8. Notably, this is the only CID process which directly corresponds to the reverse of an observed forward reaction.

The UO_3HD^- and UO_4HD^- ions exhibit disparate dissociation pathways which result in the evidently particularly stable UO_3^- ion. The different dissociation behaviors of these two ions are consistent with their disparate structures, specifically the distinctive presence of a hydridic deuterium atom in $DUO_2(OH)^-$. The elimination

Table 3. CID Products[a]

parent ion	product ion(s) and neutral(s)[b]
$U^{V}O_3HD^-$ (**2^i**)	$U^{V}O_3^-$ + HD
$U^{V}O_4CD_3H^-$ (**3^i**)	$U^{V}O_3^-$ + CD_3OH $U^{V}O_4HD^-$ + CD_2O
$U^{V}O_4C_2D_6^-$ (**4^i**)	$UO_3CD_4^-$ + CD_2O $UO_3CD_2^-$ + CD_3OD
$U^{V}O_4HD^-$ (**6^i**) $U^{VI}O_4CD_3^-$ (**8^i**) $U^{VI}O_5C_2D_6H^-$ (**9^i**) $U^{VI}O_5C_3D_9^-$ (**10^i**)	$U^{V}O_3^-$ + HDO UO_3D^- + CD_2O $U^{VI}O_4CD_3^-$ + CD_3OH $UO_4C_2D_5^-$ + CD_3OD
$U^{V}O_3{}^{18}OCH_4^-$ (**3†**)	$U^{V}O_3^-$ + $CH_3{}^{18}OH$ $U^{V}O_3H_2^-$ + $CH_2{}^{18}O$[c]
$U^{V}O_2{}^{18}O_2C_2H_6^-$ (**4†**)	$UO_2{}^{18}OCH_4^-$ + $CH_2{}^{18}O$[d] $UO_2{}^{18}OCH_2^-$ + $CH_3{}^{18}OH$
$U^{VI}O_3{}^{18}OCH_3^-$ (**8†**) $U^{VI}O_3{}^{18}O_2C_2H_7^-$ (**9†**) $U^{VI}O_2{}^{18}O_3C_3H_9^-$ (**10†**)	UO_3H^- + $CH_2{}^{18}O$ $U^{VI}O_3{}^{18}OCH_3^-$ + $CH_3{}^{18}OH$ $UO_2{}^{18}O_2C_2H_5^-$ + $CH_3{}^{18}OH$

[a] Only CID channels corresponding to loss of a single neutral are reported as these are most informative. None of the primary uranate ions, UO_2^-, UO_3^-, UO_4^- or UO_4H^-, exhibited CID under these conditions. The parent ion labeling is as shown in Scheme 2 for the deuterated products, and as described in the text for the ^{18}O products. The indicated oxidation states are based on the lowest-energy structures shown in Figure 1 and Supporting Information, Figure S4 for the parent ions; for the CID product ions, the assigned oxidation states also correspond to those of the lowest-energy computed structures, where known. [b] The indicated structures of the neutral products were not directly determined. [c] The elimination of $CH_2{}^{18}O$, which is isobaric with the alternative CH_3OH, was inferred from the CID results for **3^i**; CH_3OH loss cannot be excluded as a channel here. [d] The elimination of $CH_2{}^{18}O$, which is isobaric with alternative CH_3OH, was inferred from the CID results for **4^i**; CH_3OH loss cannot be excluded as a channel.

of only HD, and not HDO, from $DUO_2(OH)^-$, **2^i**, suggests that UO_3^-, not UO_2^-, is the preferred product, in accord with the greater abundance of the trioxide anion during the LDI ion production process.[52] The CID result for $DUO_2(OH)^-$ is in accord with the general interpretation that the inert character of UO_2^- is due to a kinetic resistance to reaction, rather than its inherent thermodynamic stability, as discussed above and seen in the computed PEPs (Supporting Information, Figures S14 and S15). The absence of UO_2^- as a CID product may also relate to the general propensity against changing oxidation states: the oxidation state in both $DUO_2(OH)^-$ and UO_3^- is U(V), whereas that in UO_2^- is U(III). The $UO_2(OH)(OD)^-$ ion, **6^i**, exclusively eliminates HDO to produce UO_3^-, this is in contrast to HD-elimination from $DUO_2(OH)^-$, which may partially reflect the greater oxidative stability of UO_3^- versus UO_4^-.

The $UO_4CD_3H^-$ ion, **3^i**, dissociates to UO_3^- (+ CD_3OH), and UO_4HD^- (+ CD_2O), where the latter ion is presumably the hydroxide deuteroxide, **6^i**. The alternative CID channel corresponding to elimination of a methanol molecule again indicates a special stability of the UO_3^- ion. CID of **3^i** was performed for the product of this composition from reaction sequences **1^i** and **2^i**. The observation that the same CID results were obtained from both provides additional confirmation that these two **3^i** species do indeed have the same structure, this being the conclusion based on the identical kinetics for reaction ***C*** in sequences ***1*** and ***2*** that the structure of **3** is the same in both. This result also supports the computed mechanisms for reactions ***B*** and ***E***, for which the products are predicted to be the same.

The structure of the UO_3D^- product from CID of $UO_4CD_3^-$, **8^i**, is not known. This product ion could reasonably be a dioxohydroxide, $DOUO_2^-$, in which the formal oxidation state is U(IV), or a trioxohydride, HUO_3^-, in which the formal oxidation state is U(VI). Conservation of oxidation states would favor the latter.

Elimination of CD_3OD from, $UO_4C_2D_6^-$, **4^i**, and $UO_5C_3D_9^-$, **10^i**, evidently produces new types of species, $UO_3CD_2^-$ from the former, and $UO_4C_2D_5^-$ from the latter. The UO_3CD_2 CID product from **4^i** could feasibly incorporate a U=CD_2 carbene bond; a $O_3U{=}CD_2^-$ trioxo carbene ion would be formally isoelectronic with the observed and evidently stable UO_4^- ion. From the PEP for reaction ***D*** (Figure 5), it is evident that the (OCH_2) ligand in the quite low-energy intermediate **II** is bound to the uranium metal center. More plausible than carbenes would be the species with a ligand known to be stable, $UO_2(OCD_2)^-$. The alternate CD_2O elimination pathway for $UO_4C_2D_6^-$, **4^i**, produces $UO_3CD_4^-$. Although the structure of this latter ion is not known, analogy with the structure of UO_3HD^-, **2^i**, suggests that it is likely either a methoxo deuteride, $DUO_2(OCD_3)^-$, or possibly a deuteroxy methide, $(D_3C)UO_2(OD)^-$. A reasonable candidate structure for the $UO_4C_2D_5^-$ CID product from **10^i** is $UO_2(OCD_3)(OCD_2)^-$.

The partially ^{18}O-substituted isotopologues, **3†**, **4†**, **8†**, **9†**, and **10†**, eliminate methanol and/or formaldehyde which incorporate an ^{18}O atom. These results are consistent with the computed mechanisms for reactions ***B***, ***C***, ***F***, ***G***, and ***H***. According to these computed mechanisms, the intact ^{18}O-labeled methoxo moiety is bonded to the uranium metal center, $U{-}{}^{18}OCH_3$. The dissociation processes then proceed by mechanisms in which the robust $U^{16}O_2$ uranyl structural unit, $^{16}O{=}U{=}{}^{16}O$, remains intact, and an ^{18}O associated with an equatorial methoxo ligand is eliminated. For example, the elimination of only species containing ^{18}O from $UO_2{}^{18}O_2C_2H_6^-$ (**4†**) supports the $UO_2(^{18}OCH_3)_2^-$ structure predicted by the computed mechanisms for reaction sequences 1 and 2. Similarly, the elimination of $CH_2{}^{18}O$ from **8†** is in accord with the expected $UO_3(^{18}OCH_3)^-$ structure. Also, the elimination of $CH_3{}^{18}OH$ from **10†** supports the computed $UO_2(^{18}OCH_3)_3^-$ structure; the uranyl motif remains intact during CID.

It is notable that only $CH_3{}^{18}OH$ and $CH_2{}^{18}O$ are eliminated from **3†**, which is formulated as $UO_2(OH)(^{18}OCH_3)^-$. This indicates that the CID decomposition pathway proceeds exclusively via elimination of the methoxo oxygen, not the hydroxo oxygen. Similarly, only $CH_3{}^{18}OH$ is eliminated from **9†**, which is formulated as $UO_2(OH)(^{18}OCH_3)_2^-$. These $CH_3{}^{18}OH$ products demonstrate reversibility in the characteristic mechanisms for the forward reactions in that the hydroxo proton is transferred to the methoxo group during the elimination processes.

The ^{18}O labeling results indicate that CID of methoxo species proceed by mechanisms which leave the C−O bond in the methoxo group intact. The ^{18}O is eliminated by either H-atom abstraction, that is, $CH_3{}^{18}OH$ elimination, or H-atom donation, that is, $CH_2{}^{18}O$ elimination.

The dissociations evidently proceed as the reverse of the forward reactions.

Where it was feasible to confidently assign oxidation states to the uranium metal center in both the parent ion and the CID product ions, that is, for parents **2**, **3**, **6**, and **9** (Table 3), it is apparent that there is no change in oxidation state upon dissociation: $U^V \rightarrow U^V/U^{VI} \rightarrow U^{VI}$. This is just as is observed for the uranate/methanol reactions (with the exception of the initial reaction of UO_4^-) and contrasts with the redox processes which occur during CID of vanadium oxide cations.[112]

Conclusions

Primary and sequential bimolecular reactions of four elementary uranium oxide (hydroxide) anions, UO_2^-, UO_3^-, UO_4^-, and UO_4H^-, with methanol were studied experimentally and theoretically. The structures of these elementary gas-phase "uranate" ions produced by LDI[52] have been computed by DFT, and these results were substantiated by experiments. The three binary oxides, including UO_4^-, have discrete U−O bonds and no O−O bonding; the UO_4H^- ion is the hexavalent uranium oxide hydroxide, $UO_3(OH)^-$. The UO_2^- ion was found to be inert, in accord with the computed PEPs for several viable reaction pathways. The other three ions each sequentially reacted with three methanol molecules, as summarized in Scheme 1, for each reaction only a single pathway and product was observed; the terminal inert products were the "uranyl" bis-methoxide, $UO_2(OCH_3)_2^-$ and the "uranyl" tris-methoxide, $UO_2(OCH_3)_3^-$. The approximately linear "uranyl" moiety in the reactant ions was retained in all of the intermediates and products. The initial step in each computed mechanism is transfer of the methanolic proton to an oxo-ligand on the uranium metal center concurrent with association of the resulting methoxy group to the uranium metal center.

Isotope labeling experiments using the CD_3OH, CD_3OD, and $CH_3{}^{18}OH$ isotopologues as reactants enabled experimental verification of several aspects of the computed mechanisms and structures, including the hydride hydroxide structure of $HUO_2(OH)^-$. The experimental results validated the efficacy of the two employed levels of density functional theory, PW91/ZORA and B3LYP/SDD, for computing PEPs and structures for reactions such as those examined in this work. The agreement between the two levels of theory was generally good, with the exceptions of energies of the intermediates and products for the UO_4^-/CH_3OH reaction. Some of the computed energies are evidently less accurate than are the mechanisms and structures. For example, the PW91/ZORA PEP for the UO_3^-/CH_3OH reaction indicates it should be endothermic by ~5 kcal mol^{-1}, and the profile for the $UO_5C_2H_7^-$ reaction includes transition states which lie above the reactant energies.

Given that a motivation for gas-phase reactivity studies is to provide a fundamental basis for understanding interfacial and condensed phase chemistry, the present results can be compared with the reaction of methanol at UO_2 solid surfaces.[62] The formation of gas-phase methoxides in the present work is evidently analogous to the initial step of methoxide formation on uranium oxide surfaces. It is also notable that CID of the hydroxide methoxide species $UO_2(OH)(OCH_3)_2^-$ results in elimination of CH_3OH; there would seem to be a correspondence of the CID results, in which the ion is essentially heated, with the recombination of adsorbed methoxy groups and hydrogen atoms upon surface heating.[62] Future gas-phase studies, both experimental and theoretical, will examine larger uranium oxide clusters and will further explore relationships of gas-phase reactions to interfacial and condensed phase chemistry.

Acknowledgment. This work was supported by the Università degli Studi della Calabria and by FP7 project HYPOMAP (project n. 233482); by Fundação para a Ciência e a Tecnologia (FCT) under contract PPCDT/QUI/58222/2004; and by the Director, Office of Science, Office of Basic Energy Sciences, Division of Chemical Sciences, Geosciences and Biosciences of the U.S. Department of Energy at LBNL, under Contract No. DE-AC02-05CH11231. M.C.M. is grateful for the opportunity to be a Guest Scientist in the Chemical Sciences Division at LBNL.

Supporting Information Available: Detailed description of the computational and experimental methods. Comparison of the bond lengths and NPA charges in a series of uranium oxides. Comparison of the reaction energetic and energy barriers computed at B3LYP/SDD and PW91/ZORA levels of theory for all the reactions studied in this work. Kinetic data plots for reactions ***A***, ***D***, and ***F***. Geometrical parameters of all of the minima and transition states involved in the studied reaction pathways (reactions ***A*** to ***H***), high-energy PEPs for the $UO_3^- + CH_3OH$ reaction, and PEPs and geometrical parameters of all of the species involved in the $UO_2^- + CH_3OH$ studied reactions. This material is available free of charge via the Internet at http://pubs.acs.org.

(112) Schröder, D.; Engeser, M.; Schwarz, H.; Rosenthal, E. C. E.; Döbler, J.; Sauer, J. *Inorg. Chem.* **2006**, *45*, 6235–6245.